A contribution of Death Induced by Survival gene Elimination (DISE) to the neurotoxicity in Alzheimer's disease

Abbreviated title: The role of DISE in Alzheimer's disease

Bidur Paudel[1,10], Si-Yeon Jeong[1,10,11], Carolina Pena Martinez[2], Alexis Rickman[2], Ashley Haluck-Kangas[1], Elizabeth T. Bartom[3,4], Kristina Fredriksen[5], Amira Affaneh[5], John A. Kessler[5], Joseph R. Mazzulli[5], Andrea E. Murmann[1], Emily Rogalski[6,7], Changiz Geula[6,7], Adriana Ferreira[8], Bradlee L. Heckmann[2], Douglas R. Green[9], Katherine R. Sadleir[5], Robert Vassar[5, 6], and Marcus E. Peter[1,3,*]

Author details

[1]Department of Medicine/Division Hematology/Oncology, [3]Department of Biochemistry and Molecular Genetics, [4]Department of Preventive Medicine/Division of Biostatistics, [5]Davee Department of Neurology, [6]Mesulam Center for Cognitive Neurology and Alzheimer's Disease, [7]Department of Psychiatry and Behavioral Sciences, [8]Department of Cell and Developmental Biology, Feinberg School of Medicine, Northwestern University, Chicago, IL 60611, [2]USF Health Byrd Alzheimer's Center and Neuroscience Institute; Department of Molecular Medicine, Morsani College of Medicine, Tampa, FL 33613, [9]Department of Immunology, St. Jude Children's Research Hospital, Memphis, TN, 38105w

[11]Current address: Ministry of Food and Drug Safety, Pharmaceutical Safety Bureau, Pharmaceutical Policy Division 187, Osongsaengmyeong 2-ro, Osong-eup, Heungdeok-gu, Cheongju-si, Chungcheongbuk-do, Republic of Korea

*Correspondence: Marcus Peter, E-mail: m-peter@northwestern.edu

[10]Shared first authorship

Keywords: DISE, Tau, neurotoxicity, RNAi

Number of pages: 26
Number of figures: 5
Number of words for abstract, introduction, and discussion: 241/795/1537

Conflict of interests

The authors declare no competing financial interests.

Acknowledgements

We would like to thank Drs. William Klein and Ruth Itzhaki for helpful discussions and input early in the project. This work was supported by National Institutes of Health grants R01NS090993 (to A.F.), R01AG030142 (to R.V.), R01AG045571, R56AG045571, R01AG067781, U19AG073153, P30AG072977, P30AG13854 (to E.R. and C.G.), R01NS124783, and L40CA231423 (to B.L.H). The content is solely the responsibility of the authors and does not necessarily represent the official views of the National Institutes of Health. Further support was provided by the McKnight Brain Research Foundation (to E.R.).

Author's contributions

MP designed experiments, analyzed data, and conceptualized the work. BP designed, performed, and analyzed most of the *in vitro* experiments and BP and S-YJ performed the Ago-RP-Seq experiments. C-PM and AR stained and imaged mouse brains. AHL generated and characterized the Drosha k.o. NB7 cells. EB developed SPOROS and EB and BP performed bioinformatics analyses. KF and AF generated and cultured human iPSC derived neurons. JK and JM provided iPSC-derived neurons and their characterizing data. AM provided conceptual input. ER and CG provided the CN, AD and SuperAger brain samples. AF provided brains from tau transgenic mice. BH and DG provided the brains of 5XFAD and 5XFAD Rubicon k.o. mice and BH performed the TUNEL staining of these brains. KS and RV provided training and input on working with AD brains. MP and BP wrote, and RV, AHK, BP, and MP edited the manuscript. All authors read and approved the final manuscript.

Abstract

Alzheimer's disease (AD) is characterized by progressive neurodegeneration, but the specific events that cause cell death remain poorly understood. Death Induced by Survival gene Elimination (DISE) is a recently discovered powerful cell death mechanism mediated by short (s) RNAs including micro (mi) RNAs acting through the RNA induced silencing complex (RISC). G-rich 6mer seed sequences in the sRNAs (position 2-7) target hundreds of C-rich seed matches in genes essential for cell survival resulting in the simultaneous activation of multiple cell death pathways. Using Argonaute precipitation and RNAseq (Ago-RP-Seq) we analyzed RISC bound sRNAs (R-sRNAs) in *in vitro* models and in the brains of multiple *in vivo* AD mouse models, aged mice, and AD patients. In *in vitro* cell line studies we find evidence for a contribution of RNAi to the toxicity by toxic Aβ42 oligomers. In addition, in AD mouse models with neurodegeneration, and in the aging brain R-sRNAs RISC bound sRNAs show a shift to more toxic seeds. In contrast, in cells that survived in post-mortem brains of AD patients and the brains of "SuperAgers", individuals over age 80 who have superior memory performance, R-sRNAs shift to more nontoxic seeds, supporting a protective function of miRNAs. Our data provide first evidence of a contribution of DISE to the neurotoxicity seen in AD suggesting that increasing the levels of protective miRNAs in the brain or blocking the activity of toxic R-sRNAs could lead to a novel way of treating the disease.

Significance Statement

This work explores a contribution of Death Induced by Survival gene Elimination (DISE), a powerful cell death mechanism based on RNA interference (RNAi) to the neurotoxicity seen in Alzheimer's disease (AD) which has solely been attributed to toxic proteins (e.g., the amyloid precursor protein or phosphorylated Tau). We show a significant association between the occurrence of toxic short (s)RNAs bound to the RNA induced silencing complex (RISC, which mediates RNAi) and the neurotoxicity seen in various AD models and patients. In addition, toxic oligomeric fragments of APP induce toxicity in part by increasing RISC bound toxic sRNAs and require the RISC component Ago2. Our work offers an alternative view on the cause of the neurotoxicity seen in neurodegenerative diseases.

Introduction

Plaques, composed of Aβ, and accumulation of hyper-phosphorylated tau protein (p-Tau) into filaments and eventually neurofibrillary tangles (NFT) are at the base of the pathology of Alzheimer's disease (AD) (Hardy and Higgins, 1992). Neuronal loss characterizes the end stage AD pathology and hence cell death has been implicated in AD. It is often associated with either inflammation (Heppner et al., 2015) and/or oxidative stress and superoxide production that can lead to neurodegeneration (Bhat et al., 2015) through activation of multiple cell death pathways (Dawson and Dawson, 2017). Toxicity by amyloid precursor protein degradation fragments such as Aβ42 is well established (Younkin, 1998) and a strong genetic association exists between early-onset familial forms of AD (FAD) and Aβ42 (Hutton et al., 1998). An RNA component has not been described to contribute to the etiology of AD.

RNA interference (RNAi) is a form of post-transcriptional regulation exerted by 19-25 nt long double stranded (ds) RNAs that negatively regulate gene expression at the mRNA level. The physiological way to induce RNAi is mostly mediated via miRNAs. They silence with the help of their seed at positions 2-7/8 of the miRNA guide strand (Lewis et al., 2003). The minimum seed length is 6 nucleotides (Lai, 2002; Lewis et al., 2003). Matching complementary regions (seed matches) predominantly located in the 3' untranslated region (3'UTR) of mRNAs are targeted (Lai, 2002) resulting in cleavage-independent translational silencing (Eulalio et al., 2008). miRNAs are transcribed in the nucleus as primary miRNA precursors (pri-miRNA) (Lee et al., 2004) which are first processed by the Drosha/DGCR8 microprocessor complex into pre-miRNAs (Han et al., 2004), and then exported from the nucleus to the cytoplasm (Yi et al., 2003). Once in the cytoplasm, Dicer/TRBP processes them further (Bernstein et al., 2001; Hutvagner et al., 2001) and these mature dsRNA duplexes are then loaded onto Argonaute (Ago) proteins to form the RNA induced silencing complex (RISC) (Wang et al., 2008). Consequently, the deletion of either Drosha or Dicer results in the loss of almost all miRNAs (Kim et al., 2016).

We previously discovered that any RISC bound short RNA (sRNA) that carries a G-rich 6mer seed can kill cells by targeting essential survival genes in a RISC and Ago2 dependent fashion ((Gao et al., 2018; Patel et al., 2022) and 6merdb.org). Cells die of simultaneous activation of multiple cell death pathways (Hadji et al., 2014). We called this phenomenon DISE (for Death Induced by Survival gene Elimination) (Putzbach et al., 2017). Consequently, the most abundant miRNAs are devoid of G-rich seeds and hence not toxic to cells (Gao et al., 2018). However, certain tumor suppressive miRNAs (e.g. miR-34a/c-5p or miR-15/16-5p) use this mechanism to kill cancer cells (Gao et al., 2018; Murmann et al., 2019). We wondered whether diseases existed in which this anticancer mechanism was overactive resulting in reduced cancer incidence but with tissue loss due to too much cell death. We focused on AD as a candidate because patients with advanced AD have lower cancer rates and late-stage cancer patients are less likely to develop dementia (Musicco et al., 2013; Majd et al., 2019; Karanth et al., 2022).

We now demonstrate that DISE may contribute to neuronal cell death in AD. Our data demonstrate that exposure of differentiated SH-SY5Y (SH) cells to Aβ42 oligomers results in an increase of RISC bound sRNAs (R-sRNAs) with more toxic seeds and that cells with reduced ability to produce most miRNAs (e.g., lacking Drosha expression) are hypersensitive to sRNAs with toxic seeds and to Aβ42. In addition, inhibiting RISC function or deletion of Ago2 reduces the toxicity of Aβ42. Supporting the contribution of DISE to neurotoxicity seen in AD we show that in two mouse models of AD with neuronal cell death, the median seed viability of R-sRNA in brains is reduced. In contrast, in postmortem brains of AD patients we found an increase in seed viability of R-sRNAs potentially due to the fact that the analyzed cells of these brains were the ones that survived years of ongoing AD and hence were more resistant to neurotoxicity. This interpretation was supported by a kinetic analysis of R-sRNAs in Aβ42-treated differentiated SH cells and in an analysis of induced pluripotent stem cell (iPSC) derived neurons from normal control and AD patients. Finally, we provide evidence for the role of miRNAs in protecting aging brains from DISE as the aging mouse brain loses expression of protective miRNAs. In addition, R-sRNAs from brains of a group of old individuals (>80 years) with memory capacity of 50-60 year-olds (SuperAgers) have a higher seed viability than R-sRNAs in the brains of age-matched control individuals. In summary, we provide first evidence of a contribution of DISE to the neurotoxicity seen in AD suggesting that increasing the levels of protective miRNAs in the brain could lead to a novel way of treating the disease.

Materials and Methods

Reagents and antibodies

The following reagents and antibodies were used (sources given in brackets): Dibutyl cyclic AMP (dbcAMP) (Sigma Aldrich #D0260), *all-trans* retinoic acid (RA) (Sigma Aldrich #R2625), Brain-derived neurotrophic factor (BDNF) (GeminiBio #300-104P), Amyloid β-Protein (Aβ42) trifluoroacetate salt (Bachem #H-8146.5000), Amyloid β-Protein (Aβ40) trifluoroacetate salt (Bachem #H-1194.5000), Aurintricarboxylic Acid (ATA) (Sigma Aldrich #189400), Opti-MeM (Thermo Fisher Scientific #31985088), Lipofectamine RNAimax (Thermofisher Scientific #56532), Lipofectamine 3000 (Thermofisher Scientific #100022052), 1,1,1,3,3,3-Hexafluoro-2-Propanol (HFIP)(Sigma Aldrich #105228), Argonaute-2 Rabbit pAb (Abcam #ab32381), Tyrosine Hydroxylase Rabbit pAb (TH)(Cell Signaling #2792), GAP43 (D9C8) Rabbit mAb (Cell Signaling #8945), Tau-1 Mouse mAb (Millipore Sigma #MAB3420), Drosha (D28B1) Rabbit mAb (Cell Signaling #3364), Goat Anti-Rabbit 2°Ab (Southern Biotech #4030-05), Goat Anti-Mouse 2°Ab (Southern Biotech #1070-05), HRP-conjugated β-Actin (C4) Mouse mAb (Santa Cruz Biotechnology #Sc-47778), Phospho-Histone H2A.X (Ser139) (20E3) Rabbit mAb (Cell Signaling #9718). Neuronal class III β tubulin (TUJ1) (mAb Covance #MMS-435P, 1:2000), LMX1A (pAb, Merck-Millipore #AB10533, 1:1000), Tyrosine Hydroxylase (pAb, Merck-Millipore #657012, 1:1000), HNF-3 beta (FOXA2) (mAb, Santa Cruz # sc-101060, 1:100).

Aβ peptide preparation

Solubilization, stock preparation and oligomerization of Aβ42 was performed as previously described (Fa et al., 2010; Stine et al., 2011) with some additional modifications. Briefly, lyophilized Aβ42 was allowed to equilibrate at room temperature for 30 min and resuspended in ice cold HFIP under fume hood to obtain 1 mM solution. To disintegrate previously formed random oligomers and achieve complete monomerization, solution was vortexed vigorously for 1 min and kept at RT for 2 hrs. After monomerization, peptide solution is aliquoted in desired volumes into 1.5 ml microcentrifuge tubes, air dried overnight and then transferred to SpeedVac for another 2 hrs to remove traces of HFIP. Complete removal of HFIP and quality of monomer formation is validated by the formation of clear peptide film observed at the bottom of the tubes. Tubes containing peptide films were parafilmed and stored at -80°C for further use. For oligomerization, tube containing peptide film is dissolved in DMSO at 5 mM, vortexed for 30 sec and sonicated in the water bath for 10 min for complete suspension. Peptide is further diluted to 100 μM, vortexed, briefly centrifuged and kept at 4°C for 24 hrs for oligomer formation. Media to dilute peptide depended on the experimental condition and lacked FBS and phenol red components. After 24 hrs low molecular weight soluble peptide oligomers were retrieved by centrifugation at 14,000g for 10 min and applied at various concentrations in toxicity assays. To control for HFIP toxicity Aβ40 was prepared in the same manner as Aβ42.

Cell culture

Human neuroblastoma cell lines; SH-SY5Y (# CRL-2266™) (SH cells) were purchased from ATCC and NB7 were kindly provided by Dr. Jill Lahti (St. Jude Children's Research Hospital, Memphis, TN). SH cells were cultured in Dulbecco's Eagle's medium (DMEM) (Corning # 10-013-CM) and NB7 cells in RPMI 160 medium (Corning # 10-040-CM), both supplemented with 10% heat inactivated fetal bovine serum (FBS) (Sigma-Aldrich # 14009C, 1% L-glutamine (Corning # 25-005-CI) and 1% penicillin/streptomycin Corning # 30-002-CI). Cells were maintained at 37°C in saturated humidity atmosphere of 95% air and 5% CO_2.

Generation of k.o. cells

NB7 Drosha k.o. cells were generated using the Alt-R CRISPR-Cas9 System (IDT DNA Technologies) following the manufacturer's protocol with the following modifications. A paired set of sgRNAs, one targeting in exon 2 (IDT predesigned gRNA Hs.Cas9.DROSHA.1.AB GUACAAAGUCUGGUCGUGGA) and one targeting downstream of exon 32 (IDT custom design AUAACUUGAUGAACAGCCAC) were annealed with the Alt-R Crispr Cas9 tracrRNA 5' ATTP 550 (#1077024) and mixed 1:1. The sRNA mix (22 pmol) was incubated with 18 pmol Alt-R Cas9 Nuclease V3 (#1081058) diluted in Resuspension Buffer R (Invitrogen #MPK10025). The Invitrogen Neon Transfection System was used to transfect the Cas9-sgRNA complex into $2x10^5$ NB7 cells in 200 mL Resuspension Buffer R with Cas9 electroporation enhancer (1200 volts, 30 ms width, 1 pulse). The next day single PE^+ cells were sorted into 96-well plates and cultured for ~ 6 weeks. SH-SY5Y Ago2 d.k.o. pool was generated by Synthego using the guide RNA sequence: UAAUUUGAUUGUUCUCCCGG. Single cells were sorted into 96-well plates with 50% conditioned media by FACS. Knockout clones were confirmed by western blot.

Cell growth and viability assessment

Transfection of all cell lines (SH, NB7 and their Drosha k.o. clones) were performed in TPP 96 well plate (Millipore Sigma # 92696) in 250 μl final volume. Briefly, 50 μl Opt-MeM containing sRNA-lipofectamine RNAiMax (NB7) or sRNA-lipofectamine 3000 (SH) complex was forward transfected to 200 μl cells containing 3,000 NB7 cells/well or 6,000 SH cells/well. The optimized amount of lipofectamine RNAiMax or lipofectamine 3000 for both cell lines was 0.3 μl. Short (s)RNAs used to transfect these cells were sNT1, sGGCAGU, sGGGGGC or sCAG (sequences all with their guide strands modified by 2'-O-methylation of their positions 1 and 2 as previously reported (Murmann et al., 2018; Patel et al., 2022)). Following transfection, cell growth was monitored for at least 160 hrs in the IncuCyte Zoom live-cell imaging system (Essen Bioscience) with a 10X objective. The cell confluency curves were generated using IncuCyte Zoom software (version 2015A). To determine the presence of metabolically active cells after various treatments, ATP quantification was performed using Cell/Titer-Glo Luminescent Cell Viability Assay Kit (Promega # G7571). Following Aβ40/Aβ42 or ATA treatment in 96 black well plate, an equal volume of Cell Titer-Glow reagent was added to the amount of cell culture media in the well. The contents were mixed in orbital shaker for 2 min to induce cell lysis and incubated for another 10 min to stabilize the luminescent signal. Subsequently, luminescence signal was recorded using microplate reader (BioTek Cytation 5).

Differentiation of SH cells

SH cells were differentiated into neuronal-like phenotypes by two methods as described previously, one by using dbcAMP (Krishtal et al., 2019) and other by the combination of retinoic acid (RA) and brain-derived neurotrophic factor (BDNF) (Encinas et al., 2000; Tagai et al., 2020). Briefly, SH cells maintained in DMEM media were seeded at a density of 10,000 cells/well in 96 black well plate. After 24 hrs, DMEM media was removed, and cells were differentiated with 1 mM dbcAMP in Nb-active no phenol red (BrainBits # NbActiv4-PR) media for 7 days. At day 5 of differentiation, undifferentiated cells were again seeded at same density in parallel. At day 7, when cells were differentiated, they were treated with 20 μM (unless otherwise noted) Aβ40/Aβ42 for 48 hrs and ATP cell viability was measured as described before. To achieve neuron-like differentiation by RA/BDNF, cells were first pre-differentiated with 10 μM RA in complete DMEM media for 5 days and then treated with 50 ng/ml BDNF in the same media that lacked FBS and phenol red for additional 2 days. Seven days differentiated neuron-like cells were then used to assess toxicity of Aβ40/Aβ42 in all experiments involving differentiated SH cells.

Hydrogen peroxide treatment

NB7 and NB7 Drosha k.o. clones (A3-3, A3-11) were seeded in 96 black well plate (3,000 cells/well) in complete RPMI media. After 24 hrs cells were treated with 25 and 50 μM H_2O_2 for 3 hrs and allowed to recover for 21 hrs and ATP cell viability was measured as described above. To validate ATP data, another 96 black well plate with similar experimental design was run in an IncuCyte machine to monitor the effect of H_2O_2 on cell proliferation (data not shown).

Aurintricarboxylic acid treatment

Stock solution of ATA was prepared in 0.1 M NaOH. Prior to sRNAs transfection or treatment with Aβ42 cells were pretreated with indicated concentrations of ATA for 2-24 hrs and its presence was continued throughout the analyses.

Reactive oxygen species (ROS) measurement

Intracellular induction of ROS was monitored by 2',7' –dichlorofluorescin diacetate (DCFDA) cellular ROS assay kit (Abcam # ab113851) in accordance with manufacturer's recommendation. Briefly, 25,000 SH cells/well were seeded at least in triplicates in 96 black well plate and differentiated for 7 days. At day 7 cells were washed once with DMEM media (devoid of phenol red and FBS) and loaded with 10 μM DCFDA for 45 min at 37°C in the dark. Following incubation, DCFDA solution was removed, washed once, and treated with 20 μM Aβ40/Aβ42 for 4 h. To evaluate ROS induction, plate was read on a microplate reader at Ex/Em =485/535 nm in end point mode in the presence of Aβ40, Aβ42 or control media. ROS induction in NB7 cells were performed in a similar manner except DCFDA incubation was done in complete RMPI no phenol red media, and the cells were washed with 1X buffer provided in the kit.

RNA extraction, reverse transcription, and quantitative real time PCR

Monolayer of 1.0 x 10^6 cells grown in 6 well plate was lysed in 500 µl/well QIAzol Lysis Reagent (Qiagen #79306) and RNA extraction was performed with QIAzol miRNeasy Mini Kit (Qiagen #217004) according to manufacturer's instruction. All RNA samples were subjected to DNAse digestion using RNAse-free DNAse set (Qiagen #79256) and eluted in 35 µl ultra-pure H_2O. RNA quality control was performed with Nanodrop 2000c spectrophotometer. Subsequently, 100 ng RNA was reverse transcribed using High-Capacity cDNA Reverse Transcription Kit (Applied Biosystems # 4368813) in 15 µl. cDNA was further diluted in ultra-pure H_2O to 45 µl, and qPCR was performed with TaqMan Universal PCR Master Mix (Thermo Fisher scientific #4324020) using 5 µl cDNA in a 20 µl total volume. Assay was run on 7500 Real Time PCR System (Applied Biosystems). Small nucleolar RNA (Z30) (Thermo Fisher Scientific, #001092) that have been reported to show good abundance and relatively stable expression was used as an endogenous control. Primers used to quantify expression levels of miRNAs in Parental and Drosha k.o. clones were hsa-miR-21 (Thermo Fisher Scientific, #0003970), Let-7a (Thermo Fisher Scientific # 000377), hsa-miR-221 (Thermo Fisher Scientific #000524) and hsa-miR-182 (Thermo Fisher Scientific #002334). Relative expression of miRNAs run in triplicates were normalized to the levels of Z30 and expressed as $2^{-\Delta\Delta Ct}$.

Western blot analysis

Cell pellets containing ~1.0 x 10^6 cells were lysed in 250 µl RIPA buffer (150 mM NaCl, 10 mM Tris HCl pH 7.2, 1% SDS, 1% TritonX-100, 1% deoxycholate, 5 mM EDTA) supplemented with 1 mM PMSF and protease inhibitor cocktail (Roche #11836170001). To ensure complete lysis, cells were kept on ice for 30 min, vortexed occasionally and sonicated. Lysed cells were then boiled for 10 min at 95°C and centrifuged (14,000 rpm at 4°C) for 15 min. Protein quantification was performed with DC Protein Assay Reagent (BIO RAD) in an iMark Microplate Reader (BIO RAD) at 750 nm. 20 µg protein per lane was run on SDS-polyacrylamide gel electrophoresis (SDS-PAGE) (BIO-RAD #1610158) at 40 mA for ~1 h. Resolved proteins were then transferred to Nitrocellulose Blotting Membrane (Healthcare #10600016) at 250 mA for 2 hrs on ice. Transferred membranes were then blocked with 5% non-fat dry milk for 1 hr at room temperature in TBST (Tris-buffered saline, 0.1% Tween 20) and immunoblotted with various antibodies overnight (1:1000 in 3% BSA in TBST). Following primary antibody incubation, membranes were washed with TBST and probed with secondary Goat-anti-Rabbit or Mouse IgG HRP (1:5000 in 1% milk for 1 hr at RT). Finally, membranes were washed and developed with Super Signal West Dura Luminol/Enhancer (Thermo Scientific #1859025).

Western blot analysis of iPSC derived midbrain dopamine neurons: Cultures were harvested at different time points as indicated in the figures and lysed in 1% Triton X-100 buffer containing protease inhibitor cocktail (Roche diagnostics, # 11-836-170-001), 1 mM PMSF, 50 mM NaF, 2 mM sodium orthovanadate by homogenization and incubation on ice for 30 minutes. The protein concentration was determined by using micro-BCA kit (ThermoFisher, # 23235) and 40 µg of lysates were loaded onto 10% Tris/glycine PAGE gels followed by transfer onto PVDF membranes (EMD Millipore, # IPFL00010) at 30V for 1hr). Membranes were post-fixed in 0.4% paraformaldehyde, washed in milliQ water and then blocked in 1:1 TBS : odyssey blocking buffer (Licor # P/N 927-40003) for 1 hr at room temperature. The membrane was incubated with primary antibodies diluted in 1:1 ratio 0.2% TBS-tween and odyssey blocking buffer overnight at 4°C. The following day the membrane was washed with 0.2% TBS-Tween and incubated with secondary antibodies for 1 hr. Anti-rabbit IgG conjugated to IRDye800 and anti-mouse IgG conjugated to Alexa 680 were used for simultaneous detection of both channels on the same blot. The blot was washed as before and scanned on an odyssey imaging system. The western blots were analyzed using Image Studio software (Licor) to quantify band intensities.

Mouse and human brain tissue

All animal experiments were approved and conducted in accordance with IACUC regulations at Northwestern University, St. Jude's Children's Hospital and University of South Florida, Tampa. 5XFAD mice were bred in house by crossing 5XFAD transgenic males (line 6799) to B6/SJL F1 hybrid females and genotyped as described (Oakley et al., 2006). Mice were sacrificed by CO_2 inhalation. One hemibrain was snap-frozen in liquid nitrogen. Three transgenic and three non-transgenic females were used for analysis. 6 or 8 months old female 5XFAD Rubicon$^{+/-}$ or 5XFAD Rubicon$^{-/-}$ mice (Heckmann et al., 2019); or 3 month old male control and Tau45-230 transgenic mice generated using the human cDNA coding sequence for tau45-230 under the control of the Thy 1.2 promoter on a C57BL/6J background (Lang et al., 2014).

Written informed consents were obtained from all human participants and the study was approved by the Northwestern University Institutional Review Board and in accordance with the Helsinki Declaration. Frozen brain tissue from the middle frontal gurus of 5 cognitively normal elderly participants, 7 clinically and pathologically confirmed AD patients (McKhann et al., 2011; Hyman et al., 2012) and three cognitive SuperAgers were obtained from the Northwestern University Alzheimer's Disease Center Brain Bank. Brains of cognitively normal

individuals were free of neurodegenerative pathology, except for age-appropriate accumulation of plaques and tangles (Hyman et al., 2012). SuperAgers participants were enrolled in the Northwestern University SuperAging Program, were 80 years or older, were required to perform on the Reys Auditory Verbal Learning test of episodic memory equal to or better than individuals 20-30 years younger, and on tests of other cognitive domains equal to or better than same-age peers (Rogalski et al., 2013) Age at death and postmortem interval were not different among the three groups ($p>0.05$). Please see Table 3-1 for characteristics of participants.

TUNEL staining of mouse brains

Brains of the indicated genotypes were harvested from mice following transcardic perfusion with 4% PFA in PBS. Harvested brains were immediately placed in 4% PFA and fixed overnight at 4°C. Brains were then briefly washed with cold PBS and transferred to 30% sucrose for cryoprotection. Brains were oriented following sagittal segmentation in OCT, sectioned, and mounted on glass slides. TUNEL staining was performed using the 594-TUNEL Assay Kit (Cell Signaling #48513) per the manufacturer's instructions. In brief, slides were rinsed in PBS to remove residual OCT medium and then permeabilized in 5% BSA/0.2% TX-100 in PBS for 30 min. Slides were washed two times in PBS then incubated for 5 min in TUNEL equilibration buffer. Next, slides were incubated for 2 hrs at 37C in TUNEL reaction mix in a humidified, dark environment. Slides were then washed 3 times in BSA/TX PBS solution above. Finally, coverslips were applied using Prolong Diamond Antifade Mountant with DAPI (Invitrogen P36931).

Slides were then imaged on a Nikon Ti-E epifluorescence microscope with Andor Clara ECCD camera and processed using Nikon Advanced Research (NIS) Elements software. Quantification of TUNEL+ cells was achieved by automatically defining and separately masking TUNEL signal and the DAPI signal using NIS Elements. TUNEL+ cells were defined where TUNEL signal was observed in the DAPI masked area using automated analysis. Automated results were subsequently verified by manual counting. TUNEL signal that was observed outside of the DAPI masked area was not included in this analysis for both automated and manual counting, although may represent additional cell death in cells that no longer stain DAPI positive.

iPSC derived excitatory forebrain neurons from an AD patient

Generation of iPSC lines from AD patients (AD1: AG5810-F [APOE3/4]; AD2: AG011414 [APOE3/4]) and healthy controls (Control 1 NUAD0635 [PBMC], Control 2: AG02261 [APOE3]) were previously described and obtained from Coriell Institute for Medical Research (Wadhwani et al., 2019) (AG5810, AG011414, AG002261) or provided by Northwestern University's Mesulam Center for Cognitive Neurology and Alzheimer's Disease (NUAD0635). iPSCs were differentiated to forebrain excitatory neurons via lentiviral-mediated overexpression of *neurogenin-2*, as previously described (Zhang et al., 2013) with minor modifications. Stem cells were maintained in mTeSR1 media (Stemcell Technologies) on Matrigel coated dishes (Corning). Upon start of differentiation, cells were single cell dissociated using Accutase (Millipore) and resuspended in mTeSR1 with 10 μM ROCK Inhibitor Y-27632 with lentiviruses encoding rrTA and pTetO-Ngn2-puro (generated by the Northwestern University Skin Biology & Diseases Resource-Based Center. The following day, medium was changed to KO-DMEM (Thermo Fisher Scientific), 1X MEM nonessential amino acids, 1X Glutamax, and 0.1% 2-mercaptoethonal, supplemented with 10 μM SB431542 (Stemgent), 100 nM LDN193189 (Stemgent), 2 μM XAV939 (Tocris Bioscience, Bristol, UK), and 3 μg/ml doxycycline (Sigma). Gradually, medium was changed over 2 days to neural induction medium, DMEM/F-12 containing MEM nonessential amino acids, Glutamax, N-2 (Thermo Fisher Scientific), D-glucose (Sigma), 2 μg/ml heparin sulfate (Sigma) supplemented with 3 μg/ml doxycycline and 2 μg/ml puromycin. Induced neurons were replated onto 6-well tissue culture plates at 450k cells/well on pre-coated with poly-L-orthnithine (Sigma), 4 μg/ml Laminin (Roche Basel, Switzerland), and 2 μg/ml Fibronectin (Sigma), cultured with neuronal maturation medium (BrainPhys Basal Medium [Stemcell Technologies], B-27 and N-2 supplements [Thermo Fisher Scientific], MEM nonessential amino acids, and Glutamax, supplemented with 3 μg/ml doxycycline and 10 ng/ml BDNF [R&D systems]). Post-plating, cells were treated with 3 μM Ara-C for 48 hrs to eliminate proliferating cells. Half of the medium was exchanged every 2 to 3 days until cell collection.

iPSC derived midbrain dopamine neurons used for *in vitro* aging study

Human iPSC from a previously characterized healthy control (line 2135 or C3 in (Mazzulli et al., 2016)) were cultured in mTeSR1 media (Stemcell Technologies) on vitronectin coated dishes. iPSCs were dissociated into single cells by accutase treatment and seeded at 5,000 cells per cm^2 in a Matrigel coated dish. Differentiation was carried out as described (Mazzulli et al., 2016) using dual SMAD inhibition followed by stimulation of sonic hedgehog and canonical WNT signaling. Cells were passaged en bloc at day 15 and then manually passed onto 10 cm dishes coated with poly-D-lysine at 66 μg/ml (Sigma # P1149) and laminin at 5 μg/ml (Roche #

11243217001). Cells were cultured in the presence of differentiation factors for 40 days, and then maintained in Neuraobasal media (Life Technologies) supplemented with Neurocult SM1 (Stemcell Technologies) and 1% penicillin / streptomycin (Life Technologies) until harvesting up to day 190.

To characterize iPSC derived neurons by immunocytochemistry, differentiated midbrain neurons were fixed in 4% paraformaldehyde in phosphate buffered saline (Life Technologies) for 20 min followed and permeabilized / blocked in PBS with 0.3% Triton X-100 containing 2% bovine serum albumin and 3% normal goat serum for 30 min. Primary antibodies were added and incubated overnight at 4°C in blocking buffer. Cells were then incubated in anti-mouse or rabbit IgG conjugated Alexa 488 (1:400) or Alexa 568 (1:200) (Life Technologies) for 1 hr, washed, then mounted in 10 μl of 4,6-diamidino-2-phenylindole dihydrochloride (DAPI)-containing Fluoromount G (Southern Biotech, #0100-20). Coverslips were analyzed by microscopy using a Leica confocal microscope (Leica TCS SPE laser at 25-50% power; CTR4000 / DMI4000B microscope) through a 10 μm section (z-series at 1 μm per section). The percentage of each cell population (FOXA2 / TH; LMX1A / βiiiTubulin) was quantified and normalized to total cell number through DAPI staining.

Ago pull-down and subsequent small RNA-seq (Ago-RP-Seq)

Ago pull down of the samples used in the study was performed as previously described (Patel et al., 2021). Briefly, frozen brain pieces from human (~250 mg, frontal cortex), mouse (~150 mg, cortex and hippocampus combined) and the cell pellets obtained from iPSC derived neurons (10^6), RA/BDNF differentiated SH cells (1.5 x 10^6), NB7 parental and Drosha k.o. clones (10^6), NB7 cells transfected with sRNAs (1.5x10^6) were lysed in 1 ml NP40 lysis buffer [50 mM Tris pH 7.5, 150 mM NaCl, 5 mM EDTA, 0.5% NP-40, 10% (v/v) glycerol, 1 mM NaF; supplemented with 1:200 EDTA-free protease inhibitors (Millipore #539134) and 1:1000 RNaisin Plus (Promega #N2615) before use]. For complete lysis, cells were kept on ice for 15 min, vortexed occasionally, and then centrifuged at 20,000g for 20 min. In the case of brain tissue samples, lysates were prepared by homogenizing tissues several times using Dounce Tissue Grinder in the same lysis buffer (Duran Wheaton Kimble # 357538). Pull down of Ago proteins (Ago 1-4) was performed by incubating 500 µg of Flag-GST-T6B peptide (Hauptmann et al., 2015) (Sigma #M8823) with 80 µl of anti-Flag M2 Magnetic beads (Sigma #M8823) at 4°C for 3 hrs in a rotor. Subsequently, beads were washed three times and resuspended in 1 ml NP40 lysis buffer. To confirm pull down of Ago proteins, 50 µl aliquot containing beads were mixed with 2x SDS-PAGE sample buffer and run on 10% SDS-PAGE gel for western blot analysis by anti-Ago2 antibody. After validation, reminder of the beads was used for RNA extraction using Trizol reagent (Ambion #15596018). Subsequently RNA pellet was resuspended in 20 µl ultra-pure H_2O and 10 µl was kept for RNA visualization purposes while another 10 µl was used for small RNA library preparation using Illumina primers (RRID:SCR_010233) as described previously (Hafner et al., 2012). Briefly, RNA was ligated with 3′-adenylated adapters using T4 RNA Ligase 2 (NEB #MO351) for 4 hrs at 16°C. Product was ethanol precipitated and run on 15% Urea-PAGE gel. To determine correct position of the ligated product in the gel, radiolabeled (^{32}P) unligated and ligated size markers (19-35nt) were also run in parallel. Ligated product was then eluted from the gel and prepared for 5' adaptor ligation. Ligation of 5' adaptor to already 3' ligated RNA product was performed with T4 RNA ligase 1 (NEB, #EL0021) at 37°C for 1 h. The product was again run on 12% Urea-PAGE gel, extracted and reverse transcribed using Superscript III reverse transcriptase (Invitrogen #18080–044). Enrichment of product was performed by amplifying cDNA with multiple rounds of few cycles PCR. Quality of cDNA was validated by bioanalyzer analysis with a single peak at ~157 bp length. Sequencing of cDNA was performed on Illumina Hi-Seq 4000. The sequence information on size markers, 3' and 5' adaptors, RT primers, and PCR primers were previously published (Patel et al., 2008).

6mer seed toxicity (SPOROS) analysis

The SPOROS pipeline (Bartom et al., 2021) was used to generate seed toxicity graphs, seed toxicity plots and seed nucleotide composition analyses. Briefly small RNAseq data sets in the form of raw fastq files were de-multiplexed, trimmed, cleaned and then compiled into a single read count table. After removing rare reads as described (Bartom et al., 2021), the remaining reads were BLASTed against lists of small RNAs from either mouse or human. Reads that matched artificial sequences in the database were removed and final raw read count table (rawCounts) was generated. The raw read count table was used to generate two read count tables; one normalized read count table (normCounts) that contained 1 million reads per sample, and the other normalized and differentially expressed read count table (differential). After annotating each count table with 6mer seed, average 6mer seed viability, miRNA, and RNA world data, various seed toxicity analyses were done. Seed toxicity graphs were generated by adding and collapsing all rows that contained same 6mer seed and RNA type and aggregating all the read counts within that 6mer seed viability in 1% bin size. Graphs were

prepared in Excel with smoothing line function on. Shown in the graphs are the peaks of normCounts plotted against % 6mer seed viability. When determining the average seed toxicity or seed composition analysis each row counts were first normalized by 1000 to ease computational complexity and the columns containing 6mer seeds and average 6mer seed viability were expanded based on the normalized read counts. Table containing frequency distribution of average 6mer viability for various groups were then used to generate basic boxplot (StatPlus (v.7.5)). Statistical analysis was done with Kruskal-Wallis test when comparing groups. Weblogo plots were generated to show average seed composition in positions 1-6. The differential expression analysis between two groups was done by taking significantly (p-value <0.05) expressed reads for each row between two groups and expressing them in delta read counts (perturbed sample-control sample). The frequency of average 6mer seed viability or 6mer seeds were then expanded based on the delta read counts to get the seed toxicity graph, seed toxicity plots, or seed toxicity compositions as described above.

Availability of data and materials

RNA seq data were deposited at GEO under accession number GSE213138 (https://www.ncbi.nlm.nih.gov/geo/query/acc.cgi?acc=GSE213138, reviewer token: ubkpguccdlsplwz). All other data generated and analyzed during this study are included in this published article and its supplementary information files.

Statistical analyses

Student's T-tests were performed in Microsoft Excel. Two-way analyses of variance were evaluated using STATA version 14.0. STATA was also used for comparing differences in polynomial distributions as described previously (Gao et al., 2018). All other statistical analyses were conducted in R version 4.0.0.

Results

Evidence for a contribution of DISE to Aβ42-induced toxicity *in vitro*

To determine whether 6mer seed toxicity could be involved in the death of brain derived cells, we chose the well characterized SH-SY5Y (SH) cell line differentiated into neurons to model neurotoxicity upon treatment with Aβ42 oligomers (Lambert et al., 1994; Feng et al., 2018; Higaki et al., 2018). Similar to other brain-derived cell lines (Patel et al., 2022), SH cells were susceptible to sRNAs that carry toxic 6mer seeds such as an sRNAs carrying the 6mer seed of miR-34a-5p (GGCAGU) (Gao et al., 2018) or the consensus toxic seed for human cells, GGGGGC (recently identified (Patel et al., 2022)) (**Fig. 1-1*A***). While sensitive, SH cells gain sensitivity to Aβ42 toxicity after differentiation (Krishtal et al., 2017). We demonstrated that our preparation of Aβ42 oligomers was more active than control nonaggregating Aβ40 in SH cells fully differentiated for 7 days either by treating them with 1 mM dbcAMP (Ferreira et al., 1990) (**Fig. 1-1*B, C***) or by using a differentiation protocol involving retinoid acid (RA) and brain-derived neurotrophic factor (BDNF) (Kaplan et al., 1993) (**Fig. 1-1*D*-*F***). After establishing the specific activity of Aβ42, we decided to use the more physiologically relevant protocol of differentiating SH cells with RA and BDNF for all subsequent experiments.

We recently reported that a minor shift in the loading of toxic sRNAs into the RISC can cause activation of DISE (Patel et al., 2021). To determine whether the toxicity of Aβ42 to SH cells was associated with a shift to more toxic RISC bound reads, we treated 7-day differentiated SH cells with Aβ42 for 2, 4, and 6 hours. We chose these time points to capture changes before the initiation of cell death, which was first detectable 24 hrs after treatment (**Fig. 1-1*F***). R-sRNA were identified by an Ago1-4 peptide pulldown, and RNA precipitation combined with high-throughput sequencing (Ago-RP-Seq) as described (Patel et al., 2021). To analyze the role of 6mer seed toxicity in disease situations we recently developed SPOROS, a semi-automated bioinformatics pipeline to analyze seed toxicity of sRNAs in a gene agnostic fashion (Bartom et al., 2021). Employing the SPOROS pipeline we found that the sRNAs that were significantly enriched in the RISC of cells treated with Aβ42 compared to cells treated with Aβ40 had a significantly lower seed viability than sRNAs that were depleted in the RISC (**Fig. 1*A***).

We postulated that normal cells are protected from 6mer seed toxicity by multiple mechanisms (Haluck-Kangas et al., 2021). One of them involves large quantities of miRNAs carrying nontoxic seeds that are expressed at high levels in normal but not cancer tissues (Lu et al., 2005; Landgraf et al., 2007; Murmann et al., 2017; Murmann et al., 2018). Consistently, we found that global downregulation of most abundant miRNAs, which carry mostly nontoxic seeds, caused by deleting either Dicer or Drosha sensitizes cells to effects of toxic sRNAs (Putzbach et al., 2017; Gao et al., 2018; Murmann et al., 2018; Putzbach et al., 2018b). We have therefore defined two criteria to assess whether a stimulus has a DISE component: 1) increased sensitivity of cells with a loss of protective miRNAs caused by deletion of the miRNA biogenesis genes Dicer or Drosha and 2) loss of activity in Ago2 deficient cells (Putzbach et al., 2017; Patel et al., 2021).

We first tested whether a brain-derived cell line would gain sensitivity to Aβ42 toxicity after deletion of Drosha. We generated Drosha knockout (k.o.) clones of the neuroblastoma cell line NB7 (**Fig. 1-2*A***). Drosha levels in two of the clones were reduced >99% resulting in about 50% reduction of RISC bound miRNAs (**Fig. 1-2*B***) (some of which are processed in a Drosha independent fashion, i.e., miR-320) with major miRNAs substantially reduced (**Fig. 1-2*C***). Previously, we characterized Drosha k.o. HCT116 cells and reported that in the absence of protective miRNA expression most R-sRNAs were not miRNAs. With Ago2 expression levels unaffected the median seed toxicity across these R-sRNAs was much higher than R-sRNAs in wt cells (Putzbach et al., 2018b). The SPOROS bioinformatics pipeline allows to visualize these changes in total and R-sRNAs and the effect of lack of Drosha expression on seed toxicity and cell fate can be quantified by producing a number of graphical outputs (Bartom et al., 2021): 1) A seed toxicity graph that plots sRNAs according to their abundance (Y axis) and seed viability (X axis), based on the average seed viability on three human cell lines (see 6merdb.org), 2) The median seed viability of all sRNAs in form of a box plot, and 3) The average nucleotide composition of the 6mer seed.

Thus, to investigate the effect of lack of Drosha on these brain derived cells, we sequenced both the total cellular and the R-sRNAs from the parental cells and two Drosha k.o. clones and analyzed the sequencing data with SPOROS (**Fig. 1-3**). Similar to the data obtained with Drosha k.o. HCT116 cells, in the two NB7 k.o. clones, many canonical miRNAs were reduced, both in the total RNA (**Fig. 1-3*A***) and the RISC bound fraction (**Fig. 1-3*D***) and other sRNAs (i.e., rRNA and tRNA fragments) were found in the RISC (**Fig. 1-3*D***). This resulted in a drop in median seed viability in both k.o. clones (**Fig. 1-3*B, E***) and resulted in a more C-rich average 6mer seed in the R-sRNA of the k.o. clones (**Fig. 1-3*F***). This result is consistent with the increase in non-miRNAs entering the RISC. We recently showed that increased loading of such toxic seed containing sRNAs primes the RISC,

rendering cells more susceptible to DISE (Patel et al., 2021). Consistent with these data, we found that the two k.o. clones were indeed much more sensitive to DISE induced by sGGCAGU (**Fig. 1-2*D***). We also found that these clones were more susceptible to H_2O_2 induced cell death (**Fig. 1-2*E***) mimicking the response to ROS which is induced in cells treated with either Aβ42 (**Fig. 1-2*F***) or toxic seed containing sRNAs (Hadji et al., 2014). After establishing that NB7 cells with reduced Drosha expression were hypersensitive to DISE, we tested whether the two k.o. clones were also more susceptible to cell death induced by Aβ42 than the parental cells. Parental NB7 cells were moderately sensitive to Aβ42 relative to Aβ40 (**Fig. 1*B***). In contrast, both Drosha k.o. clones were more sensitive to Aβ42-induced cell death consistent with the hypothesis that DISE could contribute to this form of cell death.

Next we tested the involvement of Ago2 in the toxicity elicited by Aβ42. We first used the Ago2 inhibitor aurintricarboxylic acid (ATA) (Tan et al., 2012) to determine whether toxic RNAs that kill through Ago2 showed reduced activity on RISC inhibited neuron derived cells. We treated NB7 cells with a low concentrations of ATA and showed that this inhibited DISE induced by either the two toxic seed-containing sRNAs used above or by the highly toxic Huntington's disease (HD) derived CAG trinucleotide repeat containing sRNA sCAG we recently described (Murmann et al., 2018) (**Fig. 1-4*A***). ATA inhibited toxicity induced by all three sRNAs in a dose dependent manner. Undifferentiated SH cells (used because their growth could be monitored by an IncuCyte analysis) were also protected from sCAG induced cell death by ATA (**Fig. 1-4*B***) and a rescue of sCAG induced cell death was observed in these cells (**Fig. 1-4*C***).

To determine whether ATA which at higher concentrations inhibits multiple endonucleases (Hallick et al., 1977) did indeed acts by inhibiting Ago2 and hence RNAi, we performed an Ago-RP-Seq analysis of NB7 cells transfected with either 1 nM sNT1, sGGGGGC or sGGGGGC in the presence of a low concentration of 10 μM ATA (**Fig. 1-4*D***). sGGGGGC made up ~6% of all pulled down normalized reads and the ATA treatment reduced this amount to ~0.3% (**Fig. 1-4*D***). Introduction of sGGGGGC into the cells had a substantial effect on the seed viability of the RISC bound sRNAs in these cells (**Fig. 1-4*E***). The median seed viability of sGGGGGC transfected cells dropped to 5% and ATA treatment brought this back up to 68.3% consistent with sGGGGGC no longer being toxic to the cells. This analysis confirmed the activity of ATA on Ago2 and suggested that the inhibition of the RISC uptake of the toxic sRNA is what protects the cells from transfection with sGGGGGC.

After establishing that ATA could protect cells from DISE induced by a toxic sRNA, we tested whether ATA which was previously shown to protect primary neurons from Aβ42 induced death (Loo et al., 1993) had an effect on Aβ42 induced cell death in differentiated SH cells at 10 μM (**Fig. 1*C***) a concentration sufficient to block the Aβ42 induced increase in DNA damage (**Fig. 1*D***). A small but significant reduction in cell death was observed. To exclude that the effects seen with ATA were due to inhibition of nucleases other than Ago2, we deleted Ago2 in SH cells (**Fig. 1-5**). Three clones with very low or undetectable Ago2 expression were isolated (**Fig. 1-5*A***). Ago2 deficient cells were substantially resistant to the toxicity of transfected sCAG (**Fig. 1-5*B***). We tested the sensitivity of the three Ago2 k.o. clones to the toxicity elicited by Aβ42 (**Fig. 1*E***). Undifferentiated cells were used for this experiments to prevent any effect of reduced differentiation due to impaired RISC function. Similar to the effects seen upon ATA treatment the three k.o. clones were less sensitive to Aβ42 induced toxicity than the parental cells. Together with our data on a shift to more toxic seed containing R-sRNAs in Aβ42-treated cells, these results suggested a contribution of RNAi to Aβ42-induced cell death in neuron-like cells prompting the question whether there is a contribution of DISE to the neurotoxicity seen in AD.

Reduced seed viability of R-sRNAs in the brains of AD mouse models with signs of neurotoxicity

To test whether 6mer seed toxicity could contribute to the neurodegeneration seen in AD, we first chose the widely used AD mouse model for early-onset forms of familial (F) AD, 5XFAD (Oakley et al., 2006). 5XFAD mice with the transgene driven by the Thy-1 promotor develop cerebral amyloid plaques and gliosis at two months of age, achieve high Aβ42 burden, and have reduced synaptic markers and a late neuron loss. However, these mice do not form NFTs and do not show much of an increase in staining for p-Tau (Oakley et al., 2006; Park et al., 2022) both key features of human AD. Finally, they also do not show a significant degree of neuronal cell death within the first few months (Oakley et al., 2006). No significant increase in TUNEL staining was found in brains of 6 or 8 months old mice (**Fig. 2*A, B***). We performed an Ago-RP-Seq-SPOROS analysis of cortex and hippocampus from 6 months old 5XFAD mice. A number of miRNAs were significantly differentially expressed, most notably miR-9-5p (**Fig. 2*C***). An analysis of these differentially expressed sRNAs showed that the median seed viability of all R-sRNAs was higher in the brains of 5XFAD mice compared to age-matched control mice (**Fig. 2*C***) suggesting that 6mer seed toxicity was not a driver of AD symptoms in this model, at least not at 6 months, a time at which there was little detectable cell death (**Fig. 2*A, B***).

Recently, a more aggressive model of AD was described based on the 5XFAD mice (Heckmann et al., 2019). It was shown that LC3-associated endocytosis (LANDO) in microglia is a critical regulator of immune-mediated Aβ aggregate removal and microglial activation in the 5XFAD mice. One of the gene mutations causing LANDO deficiency that were crossed into the 5XFAD background was a deletion of Rubicon. Rubicon is a gene that constrains canonical autophagy (Martinez et al., 2015). In the absence of Rubicon 5XFAD mice developed accelerated disease pathology and neurodegeneration, reactive microgliosis, tau pathology, and behavioral impairment similar to what is seen in human AD patients. A significant difference between 5XFAD and these Rubicon k.o. mice was that they develop neuronal cell death early in the disease progression (Heckmann et al., 2019) (**Fig. 2*A, B***). We compared the content of the RISC in mouse brains (cortex and hippocampus) of 6 months old 5XFAD Rubicon$^{-/-}$ mice with advanced disease to the brains of three symptom-free age-matched 5XFAD Rubicon$^{+/-}$ mice. In both genotypes miRNAs constituted >96% of the R-sRNAs. Interestingly, we again observed upregulation of miR-9-5p as seen in 5XFAD mice. However, in contrast to the 5XFAD mice, the median seed viability in the 5XFAD Rubicon$^{-/-}$ mice was significantly reduced (**Fig. 2*D***). This correlates with the increased Aβ42 levels in this model (Heckmann et al., 2019) and the resulting occurrence of cell death (**Fig. 2*A, B***).

It has been shown that Aβ toxicity is dependent on the presence of Tau. Thus, hippocampal neurons obtained from tau k.o. mice did not degenerate when cultured in the presence of aggregated Aβ (Rapoport et al., 2002; Roberson et al., 2007). Furthermore, tau depletion ameliorated Aβ-induced behavioral deficits when compared to transgenic mice overexpressing FAD-mutant amyloid precursor protein (Roberson et al., 2007). A growing body of evidence suggests that Aβ induces a series of post-translational tau modifications including its cleavage into a neurotoxic tau$_{45-230}$ fragment. High levels of this fragment were detected in human brains obtained from AD and other tauopathy subjects (Ferreira and Bigio, 2011). In addition, transgenic mice expressing tau$_{45-230}$ under the control of the Thy 1.2 promoter showed enhanced cell death of pyramidal hippocampal neurons as early as 3 months after birth, progressive synaptic loss in the hippocampus, and behavioral deficits when compared to wild type controls (Lang et al., 2014). We therefore subjected brains (hippocampi) from 3 months tau$_{45-230}$ transgenic mice (Tau tg) to the same analysis as the other two mouse models (**Fig. 2*E***). Consistent with the increase in cell death seen in this model, the median seed viability of R-sRNAs enriched or depleted in the brains of these mice was reduced by more than 10% (insert in **Fig. 2*E***). Like in the two previous AD models miR-9-5p was again strongly enriched in the RISC in the brain of these mice compared to control mice corroborating previous findings on the role of miR-9-5p in neurodegeneration (Sethi and Lukiw, 2009; Chen et al., 2021). A comparison of the data from all three mouse models suggested that the Ago-RP-Seq method reproducibly pulls down the same miRNAs from mouse brains. In fact, the majority of miRNAs that were found bound to the RISC in the three mouse models were shared between the models (miRNAs labeled in black in **Fig. 2-1**). In summary, the analysis of the R-sRNAs from the brains of three different mouse models of dementia suggest a possible contribution of 6mer seed toxicity to the neurotoxicity seen in two of the three models that show substantial neuronal cell death.

Increased seed viability of R-sRNA in Alzheimer patient brains

The data on the three AD mouse models and the *in vitro* data on SH cells suggested that a lower seed viability is associated with an increase in neurotoxicity. To determine whether this could also be found in the brains of AD patients, we compared R-sRNAs in the frontal cortex of seven postmortem AD with five control (CN = cognitive normal) brains (**Fig. 3*A*, *B***, **Table 3-1**). The age of the brain donors ranged from 77 to 93 for the AD patients and 76 to 100 for the controls. All AD cases had "high AD neuropathologic change" (Hyman et al., 2012; Montine et al., 2012). Neurofibrillary tangle stages of the selected AD patients were Braak 5-6 and Aβ plaque stages were all CERAD frequent. In the control cases, neurofibrillary tangles ranged from Braak stage 1-2 and Aβ plaques ranged from absent to frequent. Again >94% of all R-sRNAs were miRNAs supporting the efficiency of the pull down (**Fig. 3*A***). Surprisingly, AD brain RISCs were enriched in R-sRNAs with higher seed viabilities than control brains (**Fig. 3*B***). To confirm this observation, we repeated the entire library preparation and sequencing of R-sRNAs using the same Ago associated RNA previously isolated from the same brains (**Fig. 3-1*A***). The nature of the pulled down sRNAs was very similar in both experiments (**Fig. 3-1*B***). Consistent with the previous analysis we found significantly higher seed viability of R-sRNAs in AD brains than in the control brains (**Fig. 3-1*A***, right panel). This was further confirmed by isolating fresh RNA from a pair of three AD and three control brains (**Fig. 3-1*C***). While in all analyses of mouse and human AD we saw an increase in miR-9-5p, and in the human brains of miR-21-5p, the data on seed toxicity in human AD brains seemed to contradict the results obtained with two of the mouse models that showed signs of neuronal death. One interpretation of the data is that reduced seed viability of R-sRNA may only be found in a situation of ongoing neuronal loss. It is important to consider that AD develops in humans over many years and that brain regions and neurons have different

vulnerabilities to neurodegeneration (Greeve et al., 2000). Brains from human AD patients which can only be collected postmortem may only contain neurons from brain regions that were relatively resistant to the toxic environment and may have survived because they have sRNAs bound to their RISC with higher seed viability.

To test this hypothesis, we analyzed iPSC derived neurons generated from two control and two AD patients (**Fig. 3-2*A*, *B***). AD derived iPSC neurons had highly upregulated Tau1 protein and showed signs of ongoing DNA damage stress with increased H2AX phosphorylation (**Fig. 3-2*C***). The overall nature of the R-sRNAs in these iPSC derived neurons (**Fig. 3-2*D***) was similar to the one we detected in the RISC of actual human brains (**Fig. 3*A***) consistent with the neuronal nature of these cells. Interestingly, the seed viability of sRNAs bound to the RISC of AD iPSC derived neurons was significantly lower than the ones bound to the RISC of control cells (**Fig. 3-2*E***) suggesting that in cells from AD patients toxic R-sRNAs may indeed predominate.

Finally, we tested how an extended treatment of neuronal cells with Aβ42 would affect the composition of the RISC in an attempt to emulate the conditions that neurons in AD patients may be encountering. When differentiated SH cells were treated with Aβ42 for 6 hours, as expected, the median seed viability of R-sRNAs dropped (**Fig. 3*C***, left panel). In contrast, when the cells were treated for 48 hrs, a time point at which a substantial number of cells had already died, we detected an apparent increase in median seed viability of R-sRNAs in the surviving cells (**Fig. 3*C***, right panel) suggesting that chronic exposure may result in the induction of a protective response or the selection of cells with higher resistance. Interestingly, when we compared the pulled down miRNAs in seed toxicity graphs, we found that only in 48 hr stimulated cells miR-21-5p was significantly upregulated (**Fig. 3*C***, right panel). This parallels the observation that miR-21-5p was upregulated in the RISC of AD brains and is consistent with the reported protective role of this miRNA in many brain disorders, particularly in AD (Bai and Bian, 2022).

We detected specific changes in both brains from human AD patients and from mouse models of AD that suggest that 6mer seed toxicity may contribute to cell death of neurons. We do not believe that the observed difference between normal and AD brains is due to an increase in infiltrating immune cells because an analysis of neuron, glia and macrophage/lymphocyte specific miRNAs (Kosik, 2006; Rossi et al., 2011; Jovicic et al., 2013; Roy, 2016) bound to the RISC did not support that interpretation (**Fig. 3-3**). In summary, the data suggest that 6mer seed toxicity may contribute to neuronal cell death in mouse models of AD, and in the brains of human AD patients. Neurons surviving after years of disease progression may be enriched in protective miRNAs, suggesting that brain cells with toxic sRNA in the RISC that are more toxic are lost earlier during the course of the disease.

6mer seed toxicity and AD during aging

miRNAs have been shown to protect neurons from cell death (Schaefer et al., 2007; Davis et al., 2008), but aging neurons may be less able to generate miRNAs (Mori et al., 2012). Such aging neurons could be more susceptible to small RNAi active RNAs that induce cell death. To test whether aging neurons would lose their protection by nontoxic miRNAs, we compared the RISC content of the brain cells of young (2 month old) with that of old (18 month old) mice (**Fig. 4*A***). We found that the RISC in brain cells (cortex and hippocampus) of older mice contained significantly more sRNAs with low seed viability suggesting that they may be less able to protect themself against the activity of toxic sRNAs. This was independently confirmed in an analysis of another set of young and old mice (**Fig. 4-1*A*-*E***). The miRNAs that were pulled down in these two experiments were very similar (shown in black in **Fig. 4-1*A, B***), median seed viabilities of all R-sRNAs in these samples were identical (**Fig. 4-1**), and a Pearson correlation demonstrated high reproducibility between the two experiments (**Fig. 4-1*E***). Just as in experiment #1 in experiment #2 the median seed viability of the differentially expressed R-sRNA was lower in the brains of old versus young mice (**Fig. 4-1*F***).

How could aging neurons lose their protection by nontoxic miRNAs? A progressive loss of Dicer and the resultant global decrease in miRNA expression with age has been suggested as one mechanism. A study showed that Dicer expression in the brains of two year old mice is substantially reduced compared to the brains of 6 week old mice (Mori et al., 2012). We therefore wondered whether neurons with increasing age would lose expression of some of their protective miRNAs and whether sRNAs that are enriched in older neurons could be more toxic, rendering the neurons primed for DISE.

To test whether the loss of protective R-sRNAs can be seen in aged neurons *in vitro,* we tested iPSC derived neurons that were aged in a dish (Mertens et al., 2018) (**Fig. 4-2**). These cells were cultured for up to 190 days in poly-d-lysine and laminin coated dishes. We detected a substantial loss of Dicer protein with increasing age (right insert in **Fig. 4*B***). An Ago-RP-Seq-SPOROS experiment confirmed a significant decrease in seed viability of even total R-sRNAs in the five month old versus one month old iPSC derived neurons (left insert in **Fig. 4*B***).

While an analysis of brain cells from young and older individuals is not feasible, it was shown before that besides the brain another tissue whose miRNA content changes with age is spleen/immune cells (Mori et al.,

2012). Consistently, another study had reported major changes in the miRNA content of peripheral blood mononuclear cells (PBMCs) between young and old cohorts (Min et al., 2018). A reanalysis of these data for the seed viability of the differentially expressed mature miRNAs revealed a substantial drop in median seed viability in the miRNAs upregulated in the PBMCs from the old cohort (**Fig. 4*C***). This is line with our data on the mouse brains and suggests that with age different tissues may be more primed to die by DISE.

If the assumption is correct that a lower seed viability of R-sRNAs in brain cells contributes to neuronal death and dementia, then individuals that manage to maintain a high level of protective miRNAs in the RISC would be less prone to AD or other forms of dementia. To test this hypothesis, we analyzed the RISC content of brain cells from SuperAgers which are individuals age 80 and above whose episodic memory performance is at least at the level of cognitively average individuals in their 50s and 60s (Rogalski et al., 2013). We obtained brain tissue from three SuperAgers and compared them to three of our CNs of a similar age (**Table 3-1**). We did indeed find that the RISC in the SuperAger brains (average age = 90 years) contained sRNAs with a significantly higher seed viability than in control brains (average age 85.7 years) (**Fig. 4*D*, *E*** and **Fig. 4-3*A*, *B***) or even the AD brains (**Fig. 4-3*C***). These preliminary data suggest that SuperAgers have a greater resilience to the damage by toxic sRNAs which may contribute to dementia such as AD. In summary, our data are consistent with DISE contributing to the etiology of AD. Aging neurons may be more prone to this form of cell death but individuals that can maintain higher seed viability of their R-sRNAs are more resilient to AD.

Discussion

DISE was discovered as a powerful cell death mechanism (Haluck-Kangas et al., 2021). Our analysis of R-sRNAs in various AD models now supports DISE/6mer seed toxicity as a new concept of cell fate regulation that may affect the survival of neurons. While our analysis included any sRNA that can enter the RISC, in most cells including neurons >95% of the RISC content are miRNAs. The role of miRNAs in AD has been intensively studied (Pan et al., 2016; Samadian et al., 2021). Most analyses on AD associated miRNAs are based on quantifying miRNAs from total small RNA fraction and different miRNAs have been associated with the disease (Pan et al., 2016; Samadian et al., 2021). However, we and others have found that miRNAs vary dramatically in their ability to be taken up by the RISC (Flores et al., 2014; Patel et al., 2021). We therefore decided to subject various *in vitro* and *in vivo* systems as well as patient samples to an analysis of RISC bound sRNAs. We chose an Ago-RP-Seq method rather than a method involving cross-linking miRNAs with their targets, as we were not per se interested in identifying miRNA targets. We provide data on 6mer seed toxicity contributing to the neurotoxicity seen in AD.

In vitro experiments confirmed a contribution of the RISC and RNAi to the toxicity of Aβ42. In addition, we found a significant association between the level of neurotoxicity and the seed viability of R-sRNAs. Lower seed viability correlated with higher levels of cell death. Correspondingly, a higher overall seed viability of the RISC content may protect neurons from dying. The RISC in postmortem AD brains contained R-sRNAs with higher seed viability possibly due to a selection for more DISE resistant cells during the disease, consistent with the analysis of SH cells that had survived a 48 hr treatment with Aβ42. Seed viability was lower in older mouse brains and in *in vitro* aged iPSC derived neurons suggesting a loss of protective miRNAs with age. In contrast, the RISC in brain cells from SuperAgers contained significantly greater amounts of sRNAs with higher seed viability suggesting a higher resilience of these individuals against neuronal loss caused by DISE.

While inhibition or deletion of Ago2 had only a moderate effect on susceptibility of SH cells to Aβ42 induced toxicity, it points at a causal relationship between RISC status and neurotoxicity. It needs to be considered that the three other Ago proteins expressed in human cells (Ago 1, 3, and 4) which we also pulled down in our analyses play a redundant role in mediating the activity of miRNAs (Landthaler et al., 2008; Wang et al., 2012). They could therefore also be involved in binding sRNAs with toxic seeds. In fact, sRNAs other than miRNAs (i.e., tRNA and rRNA fragments) which have been identified to be increased in the brain of AD patients (Wu et al., 2021) were reported to preferentially bind to these three Ago proteins in a cross-linking, ligation, and sequencing of hybrids (CLASH) analysis (Helwak et al., 2013).

Based on our data we are now proposing a new mechanism that may explain the tissue loss seen late during the progression of AD: An age dependent imbalance between sRNAs that are toxic to neurons through RNAi and miRNAs that contain nontoxic seeds and act as protectors from 6mer seed toxicity. miRNAs may play at least two fundamental roles in most tissues: First, they regulate multiple pathways by targeting hundreds of genes, mostly involved in development and differentiation. Second, they are expressed at high levels preventing access of toxic endogenous sRNAs to the RISC.

There is ample literature to support the notion that miRNAs are neuroprotective in a number of disease models: In *Drosophila* impairing miRNA processing dramatically enhanced neurodegeneration caused by the CAG repeat gene ATXN3 (Jiang et al., 2005). We previously demonstrated how toxic CAG repeat-derived sRNAs cause cell death (Murmann et al., 2018; Murmann et al., 2022). Consistently, pathogenic ATXN3 with amplified CAG repeats showed strongly enhanced toxicity in HeLa cells after knockdown of Dicer (Bilen et al., 2006). Multiple publications on mice with a tissue specific knock-out of Dicer in brain cells showed that reducing Dicer triggers neuronal loss and causes behavioral abnormalities, followed by the premature death of the animals (see (Schaefer et al., 2007; Davis et al., 2008)). Moreover, mice with a tissue specific deletion of Dicer in spinal motor neurons exhibit hallmarks of spinal muscular atrophy (SMA) with signs of denervation (Haramati et al., 2010). Interestingly, mice with a brain specific knock out of Ago2 (using the same promoter: CaMKII Cre) showed no toxicity in neurons (Schaefer et al., 2010) suggesting that it is not the general activity of miRNAs and RNAi that is required for survival of neurons. Conversely, increasing miRNAs levels can be neuroprotective. Amyotrophic Lateral Sclerosis (ALS) disease mice treated with the antibiotic Enoxacin (Bailey and Peddie, 1985), which causes a global upregulation of miRNAs, most of them with nontoxic seeds, by stabilizing Dicer/TRBP (Shan et al., 2008; Melo et al., 2011), showed reduced disease scores (Emde et al., 2015). In addition, it was directly shown that miRNAs in Dicer knockout mice protect adult dopamine neurons from neurotoxicity (Chmielarz et al., 2017) and Enoxacin treatment promoted survival of cultured DA neurons.

It was previously reported that the brain is one of three tissues that lose most of its Dicer and consequently its miRNA expression with age (Mori et al., 2012). It is therefore possible that neurons when they age gradually lose expression of protective miRNAs rendering them susceptible to RNAi based toxicity. This toxicity could be

at the core of many degenerative diseases that affect the brain, among them AD, Parkinson's disease (PD), Huntington's disease (HD), and ALS. As this loss in humans likely occurs over decades, this would explain why so many neurodegenerative diseases have an onset during adulthood with decades of symptom-free life. Based on our data we are now proposing a new model with the RISC as a central rheostat to explain AD etiology with implications for other neurodegenerative diseases: Any 19-25 nt long sRNA when loaded into the RISC carrying a toxic 6mer seed can kill cells through DISE/6mer seed toxicity (Murmann et al., 2017; Putzbach et al., 2017; Gao et al., 2018; Putzbach et al., 2018a; Putzbach et al., 2018b) (**Fig. 5a**). Aβ oligomers (AβOs) and p-Tau can elicit a cellular response that causes upregulation of endogenous toxic sRNAs (**Fig. 5b**). Normal cells and neurons in younger individuals are protected by expressing large quantities of miRNAs (Schaefer et al., 2007; Davis et al., 2008) that carry nontoxic 6mer seeds (**Fig. 5c**). However, during aging mitochondria become dysfunctional resulting in an increase in the production of ROS (**Fig. 5d**). The stability of Dicer which is critical to miRNA expression in the brain is sensitive to ROS and interferons (IFNs) (Wiesen and Tomasi, 2009; Machitani et al., 2017) and most of its expression in the brain is lost during aging (Mori et al., 2012). During AD Aβ plaques cause further upregulation of ROS and induce inflammation resulting in elevated IFNs (**Fig. 5d**). It is highly likely that both the "killer" and the "protector" miRNAs are produced by Dicer raising the question of how protector miRNAs could be lost with age. We recently found that miRNAs with nontoxic seeds maybe preferentially modified by m6A modification (data not shown) an RNA mark that decreases with age (Min et al., 2018). In addition, it was recently shown that the highest Drosha expression in the brain is found in pyramidal neurons in the *Cornu Ammonis* (CA1-3) regions in the hippocampus and that during AD stress such as elevated ROS activates p38 MAPK which phosphorylates Drosha (Yang et al., 2015) in turn resulting in its translocation from the nucleus to the cytosol (Xu et al., 2021). This should further impair the cells ability to produce mature protective miRNAs. These events result in a vicious cycle of increasing amounts of toxic sRNAs and the progressive loss of protective miRNAs resulting in synaptic loss, neuronal dysfunction, cell death, and neurodegeneration. An age dependent loss of protective miRNAs together with the upregulation or the presence of toxic sRNAs combined with numerous genetic modifiers and genetic mutations present in familial and sporadic AD may contribute to AD.

While cell death is a component of AD, it is thought to be a relatively late event in the collection of cascades that ultimately result in symptoms. That is why many in the field do not consider cell death as being essential. However, in all models of neuronal dysfunction, whether it is hyperactivity or neuronal silence resulting in cognitive impairment, neuronal dysfunction may also lead to cell death (Zott et al., 2018). In a large and unique cell type such as a post-mitotic neuron, the disease can even affect cellular substructures as shown for developing axons due to a local activation of the RNAi machinery (Hengst et al., 2006). When patients die, they have lost a substantial amount of their brain cells. Our data support a hypothesis that high expression of nontoxic miRNAs protects from neurodegeneration and that increasing miRNA biogenesis with drugs similar to Enoxacin or blocking toxic R-sRNAs may be a viable treatment option for many neurodegenerative diseases including AD.

References

Bai X, Bian Z (2022) MicroRNA-21 Is a Versatile Regulator and Potential Treatment Target in Central Nervous System Disorders. Front Mol Neurosci 15:842288.

Bailey RR, Peddie BA (1985) Enoxacin for the treatment of urinary tract infection. N Z Med J 98:286-288.

Bartom ET, Kocherginsky M, Baudel B, Vaidyanathan A, Haluck-Kangas A, Patel M, O'Shea K, Murmann AE, Peter ME (2021) SPOROS: A pipeline to analyze DISE/6mer seed toxicity. PLOS Comp Biol 18:e1010022.

Bernstein E, Caudy AA, Hammond SM, Hannon GJ (2001) Role for a bidentate ribonuclease in the initiation step of RNA interference. Nature 409:363-366.

Bhat AH, Dar KB, Anees S, Zargar MA, Masood A, Sofi MA, Ganie SA (2015) Oxidative stress, mitochondrial dysfunction and neurodegenerative diseases; a mechanistic insight. Biomed Pharmacother 74:101-110.

Bilen J, Liu N, Burnett BG, Pittman RN, Bonini NM (2006) MicroRNA pathways modulate polyglutamine-induced neurodegeneration. Mol Cell 24:157-163.

Chen ML et al. (2021) Inhibition of miR-331-3p and miR-9-5p ameliorates Alzheimer's disease by enhancing autophagy. Theranostics 11:2395-2409.

Chmielarz P, Konovalova J, Najam SS, Alter H, Piepponen TP, Erfle H, Sonntag KC, Schutz G, Vinnikov IA, Domanskyi A (2017) Dicer and microRNAs protect adult dopamine neurons. Cell Death Dis 8:e2813.

Davis TH, Cuellar TL, Koch SM, Barker AJ, Harfe BD, McManus MT, Ullian EM (2008) Conditional loss of Dicer disrupts cellular and tissue morphogenesis in the cortex and hippocampus. J Neurosci 28:4322-4330.

Dawson TM, Dawson VL (2017) Mitochondrial Mechanisms of Neuronal Cell Death: Potential Therapeutics. Annu Rev Pharmacol Toxicol 57:437-454.

Emde A, Eitan C, Liou LL, Libby RT, Rivkin N, Magen I, Reichenstein I, Oppenheim H, Eilam R, Silvestroni A, Alajajian B, Ben-Dov IZ, Aebischer J, Savidor A, Levin Y, Sons R, Hammond SM, Ravits JM, Moller T, Hornstein E (2015) Dysregulated miRNA biogenesis downstream of cellular stress and ALS-causing mutations: a new mechanism for ALS. EMBO J 34:2633-2651.

Encinas M, Iglesias M, Liu Y, Wang H, Muhaisen A, Ceña V, Gallego C, Comella JX (2000) Sequential treatment of SH-SY5Y cells with retinoic acid and brain-derived neurotrophic factor gives rise to fully differentiated, neurotrophic factor-dependent, human neuron-like cells. J Neurochem 75:991-1003.

Eulalio A, Huntzinger E, Izaurralde E (2008) GW182 interaction with Argonaute is essential for miRNA-mediated translational repression and mRNA decay. Nat Struct Mol Biol 15:346-353.

Fa M, Orozco IJ, Francis YI, Saeed F, Gong Y, Arancio O (2010) Preparation of oligomeric beta-amyloid 1-42 and induction of synaptic plasticity impairment on hippocampal slices. J Vis Exp.

Feng MG, Liu CF, Chen L, Feng WB, Liu M, Hai H, Lu JM (2018) MiR-21 attenuates apoptosis-triggered by amyloid-beta via modulating PDCD4/ PI3K/AKT/GSK-3beta pathway in SH-SY5Y cells. Biomed Pharmacother 101:1003-1007.

Ferreira A, Bigio EH (2011) Calpain-mediated tau cleavage: a mechanism leading to neurodegeneration shared by multiple tauopathies. Mol Med 17:676-685.

Ferreira A, Busciglio J, Landa C, Caceres A (1990) Ganglioside-enhanced neurite growth: evidence for a selective induction of high-molecular-weight MAP-2. J Neurosci 10:293-302.

Flores O, Kennedy EM, Skalsky RL, Cullen BR (2014) Differential RISC association of endogenous human microRNAs predicts their inhibitory potential. Nucleic Acids Res 42:4629-4639.

Gao QQ, Putzbach WE, Murmann AE, Chen S, Ambrosini G, Peter JM, Bartom E, Peter ME (2018) 6mer seed toxicity in tumor suppressive miRNAs. Nature Comm 9:4504.

Greeve I, Hermans-Borgmeyer I, Brellinger C, Kasper D, Gomez-Isla T, Behl C, Levkau B, Nitsch RM (2000) The human DIMINUTO/DWARF1 homolog seladin-1 confers resistance to Alzheimer's disease-associated neurodegeneration and oxidative stress. J Neurosci 20:7345-7352.

Hadji A, Ceppi P, Murmann AE, Brockway S, Pattanayak A, Bhinder B, Hau A, De Chant S, Parimi V, Kolesza P, Richards JS, Chandel N, Djaballah H, Peter ME (2014) Death induced by CD95 or CD95 ligand elimination. Cell Rep 7:208-222.

Hafner M, Renwick N, Farazi TA, Mihailović A, Pena JTG, Tuschl T (2012) Barcoded cDNA library preparation for small RNA profiling by next-generation sequencing. Methods 58:164-170.

Hallick RB, Chelm BK, Gray PW, Orozco EM, Jr. (1977) Use of aurintricarboxylic acid as an inhibitor of nucleases during nucleic acid isolation. Nucleic Acids Res 4:3055-3064.

Haluck-Kangas A, Patel M, Paudel B, Vaidyanathan A, Murmann AE, Peter MP (2021) DISE/6mer Seed Toxicity - A powerful anti-cancer mechanism with implications for other diseases. J Exp Clin Cancer Res 40:389.

Han J, Lee Y, Yeom KH, Kim YK, Jin H, Kim VN (2004) The Drosha-DGCR8 complex in primary microRNA processing. Genes Dev 18:3016-3027.

Haramati S, Chapnik E, Sztainberg Y, Eilam R, Zwang R, Gershoni N, McGlinn E, Heiser PW, Wills AM, Wirguin I, Rubin LL, Misawa H, Tabin CJ, Brown R, Jr., Chen A, Hornstein E (2010) miRNA malfunction causes spinal motor neuron disease. Proc Natl Acad Sci U S A 107:13111-13116.

Hardy JA, Higgins GA (1992) Alzheimer's disease: the amyloid cascade hypothesis. Science 256:184-185.

Hauptmann J, Schraivogel D, Bruckmann A, Manickavel S, Jakob L, Eichner N, Pfaff J, Urban M, Sprunck S, Hafner M, Tuschl T, Deutzmann R, Meister G (2015) Biochemical isolation of Argonaute protein complexes by Ago-APP. Proc Natl Acad Sci U S A 112:11841-11845.

Heckmann BL, Teubner BJW, Tummers B, Boada-Romero E, Harris L, Yang M, Guy CS, Zakharenko SS, Green DR (2019) LC3-Associated Endocytosis Facilitates beta-Amyloid Clearance and Mitigates Neurodegeneration in Murine Alzheimer's Disease. Cell 178:536-551 e514.

Helwak A, Kudla G, Dudnakova T, Tollervey D (2013) Mapping the human miRNA interactome by CLASH reveals frequent noncanonical binding. Cell 153:654-665.

Hengst U, Cox LJ, Macosko EZ, Jaffrey SR (2006) Functional and selective RNA interference in developing axons and growth cones. J Neurosci 26:5727-5732.

Heppner FL, Ransohoff RM, Becher B (2015) Immune attack: the role of inflammation in Alzheimer disease. Nat Rev Neurosci 16:358-372.

Higaki S, Muramatsu M, Matsuda A, Matsumoto K, Satoh JI, Michikawa M, Niida S (2018) Defensive effect of microRNA-200b/c against amyloid-beta peptide-induced toxicity in Alzheimer's disease models. PLoS One 13:e0196929.

Hutton M, Perez-Tur J, Hardy J (1998) Genetics of Alzheimer's disease. Essays Biochem 33:117-131.

Hutvagner G, McLachlan J, Pasquinelli AE, Balint E, Tuschl T, Zamore PD (2001) A cellular function for the RNA-interference enzyme Dicer in the maturation of the let-7 small temporal RNA. Science 293:834-838.

Hyman BT, Phelps CH, Beach TG, Bigio EH, Cairns NJ, Carrillo MC, Dickson DW, Duyckaerts C, Frosch MP, Masliah E, Mirra SS, Nelson PT, Schneider JA, Thal DR, Thies B, Trojanowski JQ, Vinters HV, Montine TJ (2012) National Institute on Aging-Alzheimer's Association guidelines for the neuropathologic assessment of Alzheimer's disease. Alzheimers Dement 8:1-13.

Jiang F, Ye X, Liu X, Fincher L, McKearin D, Liu Q (2005) Dicer-1 and R3D1-L catalyze microRNA maturation in Drosophila. Genes Dev 19:1674-1679.

Jovicic A, Roshan R, Moisoi N, Pradervand S, Moser R, Pillai B, Luthi-Carter R (2013) Comprehensive expression analyses of neural cell-type-specific miRNAs identify new determinants of the specification and maintenance of neuronal phenotypes. J Neurosci 33:5127-5137.

Kaplan DR, Matsumoto K, Lucarelli E, Thiele CJ (1993) Induction of TrkB by retinoic acid mediates biologic responsiveness to BDNF and differentiation of human neuroblastoma cells. Eukaryotic Signal Transduction Group. Neuron 11:321-331.

Karanth SD, Katsumata Y, Nelson PT, Fardo DW, McDowell JK, Schmitt FA, Kryscio RJ, Browning SR, Braithwaite D, Arnold SM, Abner EL (2022) Cancer diagnosis is associated with a lower burden of dementia and less Alzheimer's-type neuropathology. Brain 145:2518-2527.

Kim YK, Kim B, Kim VN (2016) Re-evaluation of the roles of DROSHA, Exportin 5, and DICER in microRNA biogenesis. Proc Natl Acad Sci U S A 113:E1881-1889.

Kosik KS (2006) The neuronal microRNA system. Nat Rev Neurosci 7:911-920.

Krishtal J, Bragina O, Metsla K, Palumaa P, Tougu V (2017) In situ fibrillizing amyloid-beta 1-42 induces neurite degeneration and apoptosis of differentiated SH-SY5Y cells. PLoS One 12:e0186636.

Krishtal J, Metsla K, Bragina O, Tõugu V, Palumaa P (2019) Toxicity of Amyloid-β Peptides Varies Depending on Differentiation Route of SH-SY5Y Cells. J Alzheimers Dis 71:879-887.

Lai EC (2002) Micro RNAs are complementary to 3' UTR sequence motifs that mediate negative post-transcriptional regulation. Nat Genet 30:363-364.

Lambert MP, Stevens G, Sabo S, Barber K, Wang G, Wade W, Krafft G, Snyder S, Holzman TF, Klein WL (1994) Beta/A4-evoked degeneration of differentiated SH-SY5Y human neuroblastoma cells. J Neurosci Res 39:377-385.

Landgraf P et al. (2007) A mammalian microRNA expression atlas based on small RNA library sequencing. Cell 129:1401-1414.

Landthaler M, Gaidatzis D, Rothballer A, Chen PY, Soll SJ, Dinic L, Ojo T, Hafner M, Zavolan M, Tuschl T (2008) Molecular characterization of human Argonaute-containing ribonucleoprotein complexes and their bound target mRNAs. RNA 14:2580-2596.

Lang AE, Riherd Methner DN, Ferreira A (2014) Neuronal degeneration, synaptic defects, and behavioral abnormalities in tau(4)(5)(-)(2)(3)(0) transgenic mice. Neuroscience 275:322-339.

Lee Y, Kim M, Han J, Yeom KH, Lee S, Baek SH, Kim VN (2004) MicroRNA genes are transcribed by RNA polymerase II. EMBO J 23:4051-4060.

Lewis BP, Shih IH, Jones-Rhoades MW, Bartel DP, Burge CB (2003) Prediction of mammalian microRNA targets. Cell 115:787-798.

Loo DT, Copani A, Pike CJ, Whittemore ER, Walencewicz AJ, Cotman CW (1993) Apoptosis is induced by beta-amyloid in cultured central nervous system neurons. Proc Natl Acad Sci U S A 90:7951-7955.

Lu J, Getz G, Miska EA, varez-Saavedra E, Lamb J, Peck D, Sweet-Cordero A, Ebert BL, Mak RH, Ferrando AA, Downing JR, Jacks T, Horvitz HR, Golub TR (2005) MicroRNA expression profiles classify human cancers. Nature 435:834-838.

Machitani M, Sakurai F, Wakabayashi K, Takayama K, Tachibana M, Mizuguchi H (2017) Type I Interferons Impede Short Hairpin RNA-Mediated RNAi via Inhibition of Dicer-Mediated Processing to Small Interfering RNA. Mol Ther Nucleic Acids 6:173-182.

Majd S, Power J, Majd Z (2019) Alzheimer's Disease and Cancer: When Two Monsters Cannot Be Together. Front Neurosci 13:155.

Martinez J, Malireddi RK, Lu Q, Cunha LD, Pelletier S, Gingras S, Orchard R, Guan JL, Tan H, Peng J, Kanneganti TD, Virgin HW, Green DR (2015) Molecular characterization of LC3-associated phagocytosis reveals distinct roles for Rubicon, NOX2 and autophagy proteins. Nat Cell Biol 17:893-906.

Mazzulli JR, Zunke F, Isacson O, Studer L, Krainc D (2016) alpha-Synuclein-induced lysosomal dysfunction occurs through disruptions in protein trafficking in human midbrain synucleinopathy models. Proc Natl Acad Sci U S A 113:1931-1936.

McKhann GM, Knopman DS, Chertkow H, Hyman BT, Jack CR, Jr., Kawas CH, Klunk WE, Koroshetz WJ, Manly JJ, Mayeux R, Mohs RC, Morris JC, Rossor MN, Scheltens P, Carrillo MC, Thies B, Weintraub S, Phelps CH (2011) The diagnosis of dementia due to Alzheimer's disease: recommendations from the National Institute on Aging-Alzheimer's Association workgroups on diagnostic guidelines for Alzheimer's disease. Alzheimers Dement 7:263-269.

Melo S, Villanueva A, Moutinho C, Davalos V, Spizzo R, Ivan C, Rossi S, Setien F, Casanovas O, Simo-Riudalbas L, Carmona J, Carrere J, Vidal A, Aytes A, Puertas S, Ropero S, Kalluri R, Croce CM, Calin GA, Esteller M (2011) Small molecule enoxacin is a cancer-specific growth inhibitor that acts by enhancing TAR RNA-binding protein 2-mediated microRNA processing. Proc Natl Acad Sci U S A 108:4394-4399.

Mertens J, Reid D, Lau S, Kim Y, Gage FH (2018) Aging in a Dish: iPSC-Derived and Directly Induced Neurons for Studying Brain Aging and Age-Related Neurodegenerative Diseases. Annu Rev Genet 52:271-293.

Min KW, Zealy RW, Davila S, Fomin M, Cummings JC, Makowsky D, McDowell CH, Thigpen H, Hafner M, Kwon SH, Georgescu C, Wren JD, Yoon JH (2018) Profiling of m6A RNA modifications identified an age-associated regulation of AGO2 mRNA stability. Aging Cell 17:e12753.

Montine TJ, Phelps CH, Beach TG, Bigio EH, Cairns NJ, Dickson DW, Duyckaerts C, Frosch MP, Masliah E, Mirra SS, Nelson PT, Schneider JA, Thal DR, Trojanowski JQ, Vinters HV, Hyman BT, National Institute on A, Alzheimer's A (2012) National Institute on Aging-Alzheimer's Association guidelines for the neuropathologic assessment of Alzheimer's disease: a practical approach. Acta Neuropathol 123:1-11.

Mori MA, Raghavan P, Thomou T, Boucher J, Robida-Stubbs S, Macotela Y, Russell SJ, Kirkland JL, Blackwell TK, Kahn CR (2012) Role of microRNA processing in adipose tissue in stress defense and longevity. Cell Metab 16:336-347.

Murmann AE, Bartom ET, Schipma MJ, Vilker J, Chen S, Peter ME (2019) 6mer seed toxicity in viral microRNAs. iScience 23: 100737.

Murmann AE, Patel M, Jeong SY, Bartom ET, Morton AJ, Peter ME (2022) The length of uninterrupted CAG repeats in stem regions of repeat disease associated hairpins determines the amount of short CAG oligonucleotides that are toxic to cells through RNA interference. Cell Death Dis 13:1078.

Murmann AE, McMahon KM, Haluck-Kangas A, Ravindran N, Patel M, Law C, Brockway S, Wei JJ, Thaxton CS, Peter ME (2017) Induction of DISE in ovarian cancer cells in vivo. Oncotarget 8:84643-84658.

Murmann AE, Gao QQ, Putzbach WT, Patel M, Bartom ET, Law CY, Bridgeman B, Chen S, McMahon KM, Thaxton CS, Peter ME (2018) Small interfering RNAs based on huntingtin trinucleotide repeats are highly toxic to cancer cells. EMBO Rep 19:e45336.

Musicco M, Adorni F, Di Santo S, Prinelli F, Pettenati C, Caltagirone C, Palmer K, Russo A (2013) Inverse occurrence of cancer and Alzheimer disease: a population-based incidence study. Neurology 81:322-328.

Oakley H, Cole SL, Logan S, Maus E, Shao P, Craft J, Guillozet-Bongaarts A, Ohno M, Disterhoft J, Van Eldik L, Berry R, Vassar R (2006) Intraneuronal beta-amyloid aggregates, neurodegeneration, and neuron loss in transgenic mice with five familial Alzheimer's disease mutations: potential factors in amyloid plaque formation. J Neurosci 26:10129-10140.

Pan Y, Liu R, Terpstra E, Wang Y, Qiao F, Wang J, Tong Y, Pan B (2016) Dysregulation and diagnostic potential of microRNA in Alzheimer's disease. J Alzheimers Dis 49:1-12.

Park H, Lee YB, Chang KA (2022) miR-200c suppression increases tau hyperphosphorylation by targeting 14-3-3gamma in early stage of 5xFAD mouse model of Alzheimer's disease. Int J Biol Sci 18:2220-2234.

Patel M, Bartom ET, Paudel B, Kocherginsky M, O'Shea KL, Murmann AE, Peter ME (2022) Identification of the toxic 6mer seed consensus in human cancer cells. Sci Rep 12:5130.

Patel M, Wang Y, Bartom ET, Dhir R, Nephew KP, Adli M, Matei D, Murmann AE, Lengyel E, Peter ME (2021) The ratio of toxic-to-nontoxic microRNAs predicts platinum sensitivity in ovarian cancer. Cancer Res 81:3985-4000.

Patel N, Hoang D, Miller N, Ansaloni S, Huang Q, Rogers JT, Lee JC, Saunders AJ (2008) MicroRNAs can regulate human APP levels. Mol Neurodegener 3:10.

Putzbach W, Gao QQ, Patel M, Haluck-Kangas A, Murmann AE, Peter ME (2018a) DISE - A Seed Dependent RNAi Off-Target Effect that Kills Cancer Cells. Trends in Cancer 4:10-19.

Putzbach W, Haluck-Kangas A, Gao QQ, Sarshad AA, Bartom ET, Stults A, Qadir AS, Hafner M, Peter ME (2018b) CD95/Fas ligand mRNA is toxic to cells. eLife 7:e38621.

Putzbach W, Gao QQ, Patel M, van Dongen S, Haluck-Kangas A, Sarshad AA, Bartom E, Kim KY, Scholtens DM, Hafner M, Zhao JC, Murmann AE, Peter ME (2017) Many si/shRNAs can kill cancer cells by targeting multiple survival genes through an off-target mechanism. eLife 6:e29702.

Rapoport M, Dawson HN, Binder LI, Vitek MP, Ferreira A (2002) Tau is essential to beta -amyloid-induced neurotoxicity. Proc Natl Acad Sci U S A 99:6364-6369.

Roberson ED, Scearce-Levie K, Palop JJ, Yan F, Cheng IH, Wu T, Gerstein H, Yu GQ, Mucke L (2007) Reducing endogenous tau ameliorates amyloid beta-induced deficits in an Alzheimer's disease mouse model. Science 316:750-754.

Rogalski EJ, Gefen T, Shi J, Samimi M, Bigio E, Weintraub S, Geula C, Mesulam MM (2013) Youthful memory capacity in old brains: anatomic and genetic clues from the Northwestern SuperAging Project. J Cogn Neurosci 25:29-36.

Rossi RL, Rossetti G, Wenandy L, Curti S, Ripamonti A, Bonnal RJ, Birolo RS, Moro M, Crosti MC, Gruarin P, Maglie S, Marabita F, Mascheroni D, Parente V, Comelli M, Trabucchi E, De Francesco R, Geginat J, Abrignani S, Pagani M (2011) Distinct microRNA signatures in human lymphocyte subsets and enforcement of the naive state in CD4+ T cells by the microRNA miR-125b. Nat Immunol 12:796-803.

Roy S (2016) miRNA in Macrophage Development and Function. Antioxid Redox Signal 25:795-804.

Samadian M, Gholipour M, Hajiesmaeili M, Taheri M, Ghafouri-Fard S (2021) The Eminent Role of microRNAs in the Pathogenesis of Alzheimer's Disease. Front Aging Neurosci 13:641080.

Schaefer A, O'Carroll D, Tan CL, Hillman D, Sugimori M, Llinas R, Greengard P (2007) Cerebellar neurodegeneration in the absence of microRNAs. J Exp Med 204:1553-1558.

Schaefer A, Im HI, Veno MT, Fowler CD, Min A, Intrator A, Kjems J, Kenny PJ, O'Carroll D, Greengard P (2010) Argonaute 2 in dopamine 2 receptor-expressing neurons regulates cocaine addiction. J Exp Med 207:1843-1851.

Sethi P, Lukiw WJ (2009) Micro-RNA abundance and stability in human brain: Specific alterations in Alzheimer's disease temporal lobe neocortex. Neuroscience Letters 459:100-104.

Shan G, Li Y, Zhang J, Li W, Szulwach KE, Duan R, Faghihi MA, Khalil AM, Lu L, Paroo Z, Chan AW, Shi Z, Liu Q, Wahlestedt C, He C, Jin P (2008) A small molecule enhances RNA interference and promotes microRNA processing. Nat Biotechnol 26:933-940.

Stine WB, Jungbauer L, Yu C, LaDu MJ (2011) Preparing synthetic Abeta in different aggregation states. Methods Mol Biol 670:13-32.

Tagai N, Tanaka A, Sato A, Uchiumi F, Tanuma SI (2020) Low Levels of Brain-Derived Neurotrophic Factor Trigger Self-aggregated Amyloid β-Induced Neuronal Cell Death in an Alzheimer's Cell Model. Biol Pharm Bull 43:1073-1080.

Tan GS, Chiu CH, Garchow BG, Metzler D, Diamond SL, Kiriakidou M (2012) Small molecule inhibition of RISC loading. ACS Chem Biol 7:403-410.

Wadhwani AR, Affaneh A, Van Gulden S, Kessler JA (2019) Neuronal apolipoprotein E4 increases cell death and phosphorylated tau release in alzheimer disease. Ann Neurol 85:726-739.

Wang D, Zhang Z, O'Loughlin E, Lee T, Houel S, O'Carroll D, Tarakhovsky A, Ahn NG, Yi R (2012) Quantitative functions of Argonaute proteins in mammalian development. Genes Dev 26:693-704.

Wang Y, Sheng G, Juranek S, Tuschl T, Patel DJ (2008) Structure of the guide-strand-containing argonaute silencing complex. Nature 456:209-213.

Wiesen JL, Tomasi TB (2009) Dicer is regulated by cellular stresses and interferons. Mol Immunol 46:1222-1228.

Wu W, Lee I, Spratt H, Fang X, Bao X (2021) tRNA-Derived Fragments in Alzheimer's Disease: Implications for New Disease Biomarkers and Neuropathological Mechanisms. J Alzheimers Dis 79:793-806.

Xu H, Liu X, Li W, Xi Y, Su P, Meng B, Shao X, Tang B, Yang Q, Mao Z (2021) p38 MAPK-mediated loss of nuclear RNase III enzyme Drosha underlies amyloid beta-induced neuronal stress in Alzheimer's disease. Aging Cell 20:e13434.

Yang Q, Li W, She H, Dou J, Duong DM, Du Y, Yang SH, Seyfried NT, Fu H, Gao G, Mao Z (2015) Stress induces p38 MAPK-mediated phosphorylation and inhibition of Drosha-dependent cell survival. Mol Cell 57:721-734.

Yi R, Qin Y, Macara IG, Cullen BR (2003) Exportin-5 mediates the nuclear export of pre-microRNAs and short hairpin RNAs. Genes Dev 17:3011-3016.

Younkin SG (1998) The role of A beta 42 in Alzheimer's disease. J Physiol Paris 92:289-292.

Zhang Y, Pak C, Han Y, Ahlenius H, Zhang Z, Chanda S, Marro S, Patzke C, Acuna C, Covy J, Xu W, Yang N, Danko T, Chen L, Wernig M, Sudhof TC (2013) Rapid single-step induction of functional neurons from human pluripotent stem cells. Neuron 78:785-798.

Zott B, Busche MA, Sperling RA, Konnerth A (2018) What Happens with the Circuit in Alzheimer's Disease in Mice and Humans? Annu Rev Neurosci 41:277-297.

Figure legends

Figure 1. Aβ42 is toxic to differentiated SH cells in part through 6mer seed toxicity. ***A,*** Difference in seed viability of R-sRNAs significantly ($p<0.05$) under- or overrepresented in 7 day differentiated SH cells treated with Aβ42 for different periods of times (compared to Aβ40 treated cells). Shown are the medians and Kruskal-Wallis median test p-values. ***B,*** Viability assay of parental NB7 cells or two Drosha k.o. clones after a 48 hr treatment with Aβ40 or Aβ42. ***C,*** Viability assay of differentiated SH cells treated for 72 hrs with either 10 μM Aβ40 or Aβ40 in the absence or presence of 10 μM ATA. ***D,*** Western blot for γH2AX of 7 day differentiated SH cells treated with Aβ40 or Aβ42 for four hours in the absence or pretreated for 24 hrs with of 10 μM ATA. ***E,*** Viability assay of three Ago2 k.o. SH clones after exposure to 20 μM Aβ40 or Aβ42 for 72 hrs. Mean with SD and Student's t-test p-values are shown (***B, C, E***).

Figure 1-1. Differentiated SH cells are more sensitive to the toxicity of Aβ42. ***A,*** Change in confluence over time of SH cells treated with lipid only or transfected with 10 nM of the indicated sRNA. Data points are from triplicates and mean -/+ SE. ***B,*** Western blot analysis of SH cells cultured in DMEM or in NB-active medium with and without dbcAMP. TH, tyrosine hydroxylase. ***C,*** Viability assay of dbcAMP day 1 or day 7 differentiated SH cells left untreated or treated with either Aβ40 or Aβ42 for 48 hrs. Data are in triplicate. Shown is the mean with SD and Student's t-test p-values. ***D,*** Phase contrast image of undifferentiated SH cells or SH cells differentiated with RA/BDNF for 7 days. Size bar = 60 μm. ***E,*** Western blot analysis of cells in ***D***. ***F,*** Viability of undifferentiated or 7 day differentiated SH cells treated with either Aβ40 or Aβ42 for 24 or 48 hrs. Data were normalized to the 24 hr treatment with Aβ40.

Figure 1-2. Generation and characterization of Drosha k.o. NB7 cells. ***A,*** Western blot analysis of parental NB7 cells and two Drosha k.o. clones. Densitometrical quantification of Drosha relative to Actin is shown. Par, parental. ***B,*** Relative amounts of total RISC bound miRNAs of the cells in a. ***C,*** Real-time PCR quantification of major miRNAs in the two k.o. clones relative to parental cells. Shown are averages with variance of samples done in duplicate (miR-221/miR-181) or SD of samples done in triplicate (Let-7a and miR-21). The data on miR-21 and Let-7a are representative of two biological replicates. ***D,*** Change in confluence over time of NB7 parental cells or two Drosha k.o. clones treated with lipid only or transfected with 1 nM of siGGCAGU. Data points are from triplicates and mean -/+ SE. P-values were calculated using a polynomial distribution test and support a difference in sensitivity between parental NB7 and the two Drosha k.o. clones. ***E,*** Viability assay of parental and two Drosha k.o. clones 24 hrs after a 3 hr treatment with 25 or 50 μM H_2O_2. ***F,*** Quantification of ROS levels of NB7 cells left untreated or treated with Aβ40 or Aβ42.

Figure 1-3. SPOROS analysis of total and RISC bound sRNAs in Drosha k.o. NB7 cells. ***A,*** Seed toxicity graph of all sRNAs sequenced in parental NB7 cells and two Drosha k.o. clones. sRNAs with 10,000 or more reads in at least one sample are labeled. Enriched sRNAs are shown in green and depleted sRNAs in red. ***B,*** Seed toxicity plots of the seed viability of the samples in ***A***. Shown are the medians and Kruskal-Wallis median test p-value. ***C,*** Average seed composition of all sRNAs in the three samples in ***A***. ***D,*** Seed toxicity graph of all R-sRNAs sequenced in parental NB7 cells and two Drosha k.o. clones. sRNAs with 10,000 or more reads in at least one sample are labeled. Enriched sRNAs are shown in green and depleted sRNAs in red. ***E,*** Seed toxicity plots of the seed viability of the samples in ***D***. Shown are the medians and Kruskal-Wallis median test p-value. ***F,*** Average seed composition of all sRNAs in the three samples in ***D***.

Figure 1-4. ATA blocks RISC uptake of DISE-inducing sRNAs and protects from DISE in NB7 and SH cells. ***A,*** Change in confluence over time of NB7 cells treated with lipid only or transfected with the indicated sRNA in the absence or presence of increasing concentrations of ATA. Data points are from triplicates and mean -/+ SE. ***B,*** Change in confluence over time of SH cells treated with lipid only or transfected with 5 nM of sCAG in the absence or presence of 5 μM ATA. Data points are from triplicates and mean -/+ SE. ***C,*** Viability assay of differentiated SH cells 72 hrs after treatment with either lipid or 5 nM of sNT1 or sCAG in the absence of presence of 10 μM ATA. Student's ttest p-value is shown for the comparison between cells treated with sNT1 versus sCAG. ***D,*** Counts (normalized to 1 million reads) of the sGGGGGC antisense strand in the RISC of NB7 cells transfected with either 1 nM sNT1, sGGGGGC or sGGGGGC and treated with 10 μM ATA. Shown are the averages of biological triplicates -/+ SD. The percent of the sRNA in the total R-sRNA is given for the sGGGGGC transfected cells. ***E,*** Seed toxicity plots with the seed viability of the differentially expressed R-sRNAs of the samples in ***C***. *Left:* comparison of the reads in sNT1 and sGGGGGC transfected cells; *right:* comparison of the reads in

sGGGGGC transfected cells minus/plus ATA. Shown are the medians and Kruskal-Wallis median test p-value between indicated samples.

Figure 1-5. Generation and characterization of Ago2 k.o. SH cells. ***A,*** Western blot analysis of parental SH cells and three Ago2 k.o. clones. ***B,*** Change in confluence over time of SH parental and Ago2 k.o. cells treated with lipid only or transfected with 5 nM of the indicated sRNAs. Data points are from triplicates and mean -/+ SE.

Figure 2. Reduction in seed viability of R-sRNAs in AD mouse models with neurotoxicity. ***A,*** Representative TUNEL staining of brains of 6 months old control ($5XFAD^{Neg}$/$Rubicon^{+/-}$ and $5XFAD^{Neg}$/$Rubicon^{-/-}$), 5XFAD tg ($5XFAD^{TG}$/$Rubicon^{+/-}$), and $5XFAD^{TG}$/$Rubicon^{-/-}$ mice. Brain sections were counterstained with DAPI. Size marker = 200 μm. ***B,*** Quantification of TUNEL positivity in brains of mice with four different genotypes. *Top,* 6-months and *bottom*, 8-months old mice. Student's T-test p-values are given. ns, not significant. ***C, D, E,*** Seed toxicity graphs of differentially expressed R-sRNAs ($p<0.05$) between Ctr and 5XFAD (***C***), 5XFAD $Rubicon^{+/-}$ (Het) and 5XFAD $Rubicon^{-/-}$ (***D***), control and Tau tg (***E***) brains. miRNAs are labeled that have a difference in expression of 1000 or more reads. Enriched sRNAs are shown in green and depleted sRNAs in red. Shown are averages of triplicate (***C, E***) or quadruplicate (***D***) samples. Inserts: Seed toxicity plots of the seed viability of the same samples. Shown are the median viability of opposing differentially expressed and/or RISC-loaded sRNAs. Kruskal-Wallis median test p-value are given.

Figure 2-1. SPOROS analysis of total sRNAs in three AD mouse models. ***A, C, E,*** Seed toxicity graph of total R-sRNAs of Ctr and 5XFAD (***A***), 5XFAD $Rubicon^{+/-}$ and 5XFAD $Rubicon^{-/-}$ (***C***) and Ctr and Tau tg (***E***) brains. Shown are averages of triplicate (***A*** and ***E***) and quadruplicate (***C***) samples. In all cases sRNAs with 10,000 or more reads in at least one sample are labeled. In each label sRNAs are listed in the order of expression levels. sRNAs shared in all three analyses are shown in black. ***B, D, F,*** *Top*, Seed toxicity plots of the total seed viability of the samples in **A, C** and **E**. Medians and Kruskal-Wallis median test p-value are given. *Bottom*, average seed composition of the sRNAs in the same samples.

Figure 3. Increased seed viability of R-sRNA in postmortem human Alzheimer patient brains and differentiated SH cells treated with Aβ42 for 2 days. ***A, B,*** Seed toxicity graphs of total R-sRNAs (A) and differentially expressed R-sRNAs (***B***) of CN and AD brains. Shown are averages of 5 (CN) and 7 (AD) samples (experiment #1). ***C,*** Seed toxicity graphs of differentially expressed R-sRNAs of 7 day differentiated SH cells treated with either Aβ40 or Aβ42 for 6 hrs (left) or 48 hrs (right). Shown are averages of 2 samples. sRNAs with 10,000 or more reads in at least two samples (***A***) or that have a difference in expression of 1000 or more reads (***B, C***) are labeled. In each label sRNAs are listed in the order of expression levels. Enriched sRNAs are shown in green and depleted sRNAs in red. Inserts: Seed toxicity plots of the differential seed viability of each analysis. Medians and Kruskal-Wallis median test p-value are given.

Figure 3-1. Repeat analyses of human postmortem AD brains using SPOROS**.** ***A,*** *Left:* Seed toxicity graph of differentially expressed R-sRNAs of CN and AD brains. Shown are averages of 5 (CN) and 7 (AD) samples (experiment #2). Enriched sRNAs are shown in green and depleted sRNAs in red. sRNAs that have a difference in expression of 1000 or more reads are labeled and, in each label, sRNAs are listed in the order of expression levels. *Right:* Seed toxicity plot of the differential seed viability of the analysis. Medians and Kruskal-Wallis median test p-value are given. ***B,*** Pearson correlation analyses of gene products covered by the reads immunoprecipitated in the experiments shown in Fig. 3A (Exp #1) and in ***A*** (Exp #2). Only genes were included with an average of 10 reads across all samples. ***C,*** Seed toxicity graphs of differentially expressed R-sRNAs (***A***) of 3 CN and 3 AD brains. Medians and Kruskal-Wallis median test p-value are given.

Figure 3-2. Reduced seed viability of R-sRNAs in iPSC derived neurons from AD patients. ***A,*** Bright field image of the NGN2 excitatory neurons derived from two control and two AD patients 36 days post differentiation. Size bar = 500 μm. ***B,*** Immunofluorescence images of the AD derived neurons using the neuronal marker βiiiTubulin and the glutamatergic neuronal marker vesicular glutamate transporter (vGLUT) counterstained with DAPI. Size bar = 50 μm. ***C,*** Western blot analysis of Ctr (NUAD0635) and AD (AG5810) iPSC derived neurons. The analysis was done with half of the cells that were subjected to the Ago-RP-Seq-SPOROS analysis. ***D,*** Seed toxicity graph of total R-sRNAs of the two Ctr and two AD patient derived iPSC derived neurons (average for each set is shown). Shown are averages of duplicate samples. sRNAs with 10,000 or more reads in at least one sample are labeled. In each label sRNAs are listed in the order of expression levels. ***E,*** *Top*, Seed toxicity plot of the

differential seed viability of the samples in A. Medians and Kruskal-Wallis median test p-value are given. *Bottom*, average seed composition of the sRNAs in the same samples.

Figure 3-3. Total read numbers of neuron, glia and immune cell specific RISC bound miRNAs in different brain samples. Normalized expression levels of miRNAs pulled down in different tissues in the three experiments described in Fig. 3*D*, 2*B*, and 2*E*. Shown are averages with SD. None of the comparisons between ctr and respective AD model reached statistical significance.

Table 3-1. Description of all patient brain material used. CN = Cognitive normal; AD = Alzheimer's disease confirmed by neuropathologist; SA = SuperAger; T = Temporal Cortex; O = Occipital Cortex; F = Female; M = Male; F = Female; PMI = Postmortem Interval, C = Caucasian; Fr = Fresh; ADNC = Alzheimer's Disease Neuropathologic Change. In blue font: Used in Fig. 3*A*, *B* and Supplementary Fig. 3-1*C*.

Figure 4. Changes in seed viability of R-sRNAs with age. ***A,*** Seed toxicity graph of differentially expressed R-sRNAs of 2 months and 18 months old mouse brains. Shown are averages of triplicate samples. sRNAs that have a difference in expression of 1000 or more reads are labeled. Enriched sRNAs are shown in green and depleted sRNAs in red. Insert: Seed toxicity plot of the differential seed viability of the analysis. Medians and Kruskal-Wallis median test p-value are given. ***B,*** Seed toxicity graph of total R-sRNAs of iPSC derived neurons aged for 1 and 5 months. sRNAs with 10,000 or more reads in at least one sample are labeled. In each label sRNAs are listed in the order of expression levels. Enriched sRNAs are shown in green and depleted sRNAs in red. Insert: Seed toxicity plot of the differential seed viability of the analysis. Medians and Kruskal-Wallis median test p-value are given. Western blot insert: Analysis of iPSC derived neurons aged *in vitro* for 30, 150 or 190 days. Densitometrical quantification relative to the 30-day time point and actin is given. ***C,*** *Top*, Average seed toxicity of all significantly up- and downregulated miRNAs in PBMCs of old versus young donors (Min et al., 2018). *Bottom*, Nucleotide composition at each of the six seed positions in the miRNAs analyzed above. ***D,*** Seed toxicity graph of differentially expressed R-sRNAs of postmortem CN and SuperAger brains. Shown are averages of triplicate samples. sRNAs that have a difference in expression of 1000 or more reads are labeled. In each label sRNAs are listed in the order of expression levels. Enriched sRNAs are shown in green and depleted sRNAs in red. Age of the three CN participants: 100, 87, 83 - average = 90, age of the three SuperAgers: 82, 85, 90 - average = 85.7. ***E,*** *Top*, Seed toxicity plots of the differential seed viability of the samples in ***D***. Medians and Kruskal-Wallis median test p-value are given. *Bottom*, average seed composition of the sRNAs in the same samples.

Figure 4-1. Repeat analysis of young and old mouse brains using SPOROS. ***A, B,*** Seed toxicity graph of total R-sRNAs of 2 months and 18 months old mouse brains. Experiment #1 (***A***) and Experiment #2 (***B***). Shown are averages of triplicate (***A***) and duplicate (***B***) samples. In all cases sRNAs with 10,000 or more reads in at least one sample are labeled. In each label sRNAs are listed in the order of expression levels. sRNAs shared in all three analyses are shown in black. ***C, D,*** *Top*, Seed toxicity plots of the total seed viability of the samples in ***A*** and ***B***. Medians and Kruskal-Wallis median test p-value are given. *Bottom*, average seed composition of the sRNAs in the same samples. ***E,*** Pearson correlation analysis of gene products covered by the reads precipitated in the experiments shown in ***A*** (Exp #1) and in ***B*** (Exp #2). Only genes were included with an average of 10 reads across all samples. ***F,*** Seed toxicity plot of differentially expressed R-sRNAs of 2 months and 18 months old mouse brains (Exp. #2). Medians and Kruskal-Wallis median test p-value are given.

Figure 4-2. Characterization of human iPSC-derived midbrain dopamine neurons that were aged *in vitro*. ***A,*** Brightfield image of iPSCs before differentiation (day 0). ***B,*** Immunostaining analysis of midbrain dopamine (DA) neurons at day 75 using antibodies that detect neuronal (βiii Tubulin) or DAergic specific markers (LMX1A, FOXA2, Tyrosine Hydroxylase (TH). DAPI (Blue) was used to stain nuclei. ***C,*** Western blot analysis of DAergic markers TH, βiiiTubulin. Non-neuronal GAPDH was used as loading control. ***D,*** Western blot analysis of βiiiTubulin normalized to GAPDH, quantified on the right documents the stability on the culture system over time.

Figure 4-3. SPOROS analysis of all R-sRNAs in brains of SuperAgers. ***A,*** Seed toxicity graph of total R-sRNAs of postmortem CN and SuperAger brains. Shown are averages of triplicate samples. In all cases sRNAs with 10,000 or more reads in at least one sample are labeled. In each label sRNAs are listed in the order of expression levels. ***B,*** *Top*, Seed toxicity plots of the total seed viability of the samples in ***A***. *Bottom*, average seed composition of the sRNAs in the same samples. Medians and Kruskal-Wallis median test p-value are given. ***C,***

Seed toxicity plots of differential seed viability of postmortem SuperAger versus AD brains. Medians and Kruskal-Wallis median test p-value are given.

Figure 5. A model on the role of 6mer seed toxicity in AD. **a,** The executioner: The RISC with bound sRNAs carrying toxic 6mer seeds causing induction of DISE. **b,** The killers: Stimuli that cause the increase in toxic sRNAs in neurons above the level that the protectors can buffer. **c,** The protectors: A miRNA-based mechanism that protects normal neurons from toxic sRNAs by blocking their access to the RISC. **d,** The modifiers: Stimuli that cause the loss of protection of neurons and during stress and aging exposing cells to the toxic sRNAs. RISC, RNA-induced silencing complex; DISE, death induced by survival gene elimination; sRNA; short RNA; IFN, proinflammatory cytokines including interferons; AGOs, Argonaute proteins, critical components of the RISC; ROS, reactive oxygen species. Two inhibitors and their site of action are shown. Green line, neuron plasma membrane; blue line, neuron nucleus.

Figure 1

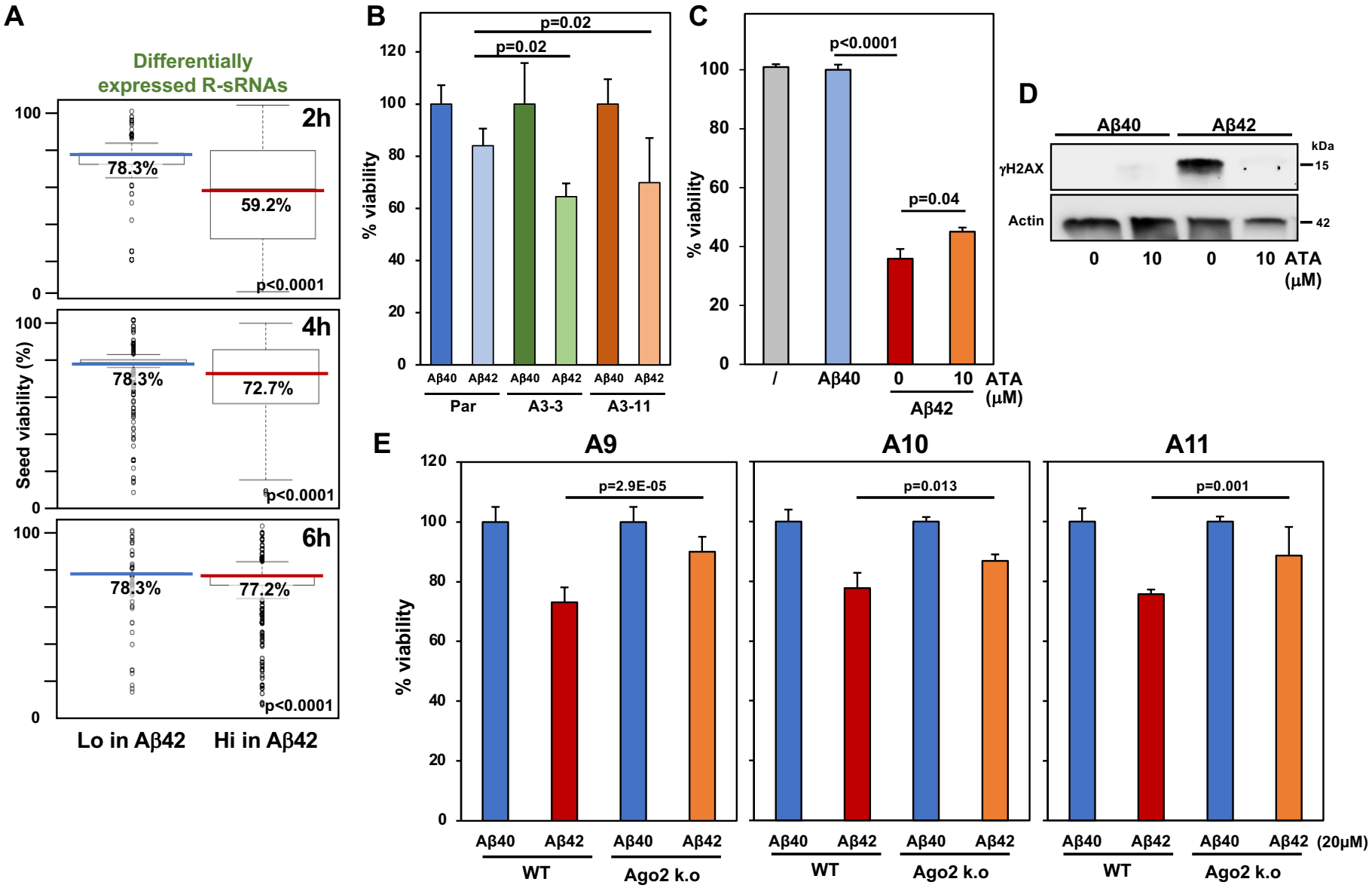
A
Differentially expressed R-sRNAs
2h
78.3%
59.2%
p<0.0001
4h
78.3%
72.7%
p<0.0001
6h
78.3%
77.2%
p<0.0001
Seed viability (%)
Lo in Aβ42
Hi in Aβ42
B
p=0.02
p=0.02
% viability
Aβ40 Aβ42 Aβ40 Aβ42 Aβ40 Aβ42
Par
A3-3
A3-11
C
p<0.0001
p=0.04
% viability
/
Aβ40
0
10
ATA (μM)
Aβ42
D
Aβ40
Aβ42
kDa
γH2AX
15
Actin
42
0 10 0 10 ATA (μM)
E
A9
A10
A11
p=2.9E-05
p=0.013
p=0.001
% viability
Aβ40 Aβ42 Aβ40 Aβ42
WT
Ago2 k.o
(20μM)

Figure 1-1

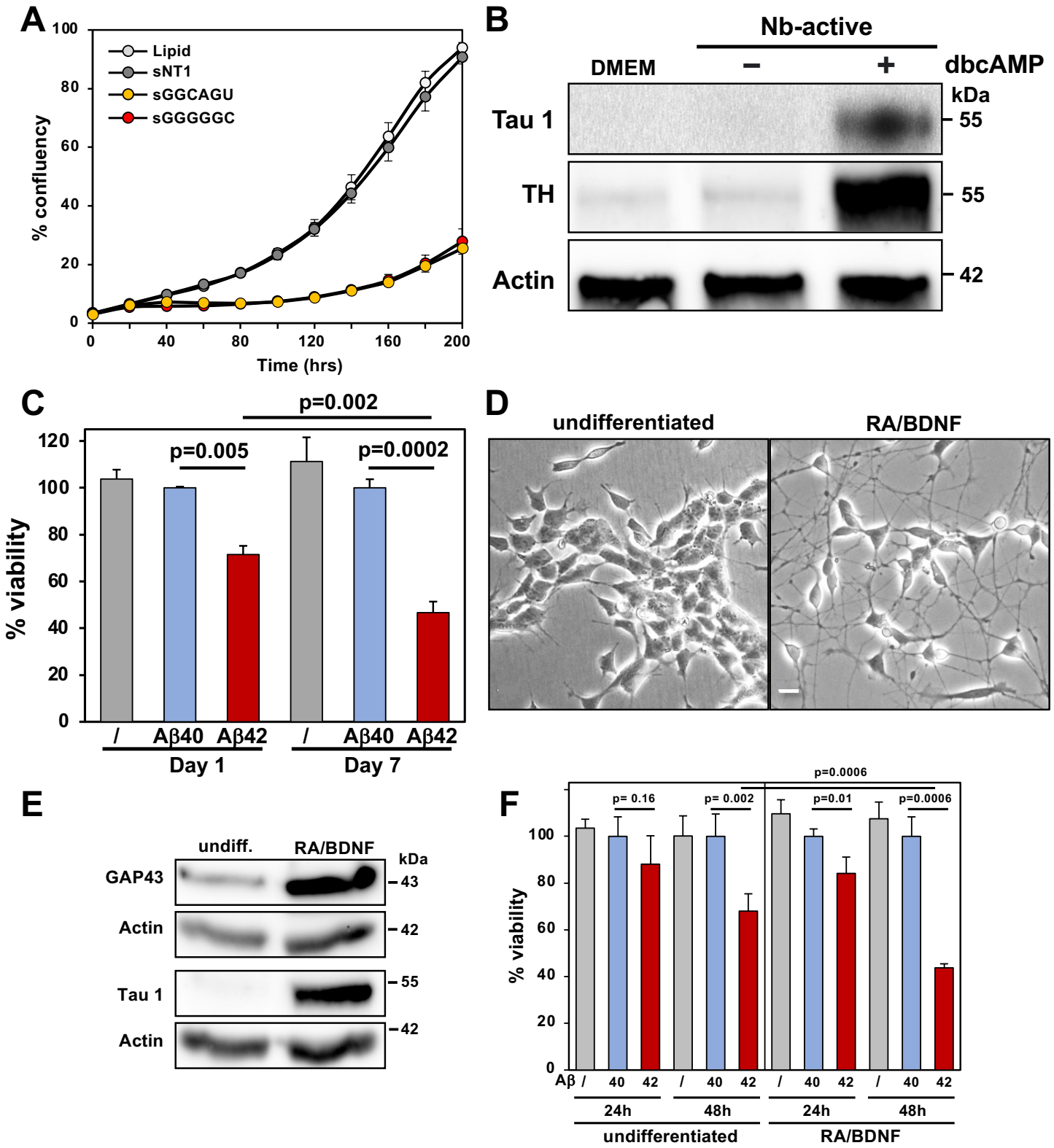
A
Lipid
sNT1
sGGCAGU
sGGGGGC
% confluency
Time (hrs)
B
Nb-active
DMEM
−
+
dbcAMP
kDa
Tau 1
TH
Actin
55
55
42
C
p=0.002
p=0.005
p=0.0002
% viability
/
Aβ40
Aβ42
Day 1
Day 7
D
undifferentiated
RA/BDNF
E
undiff.
RA/BDNF
kDa
GAP43
Actin
Tau 1
Actin
43
42
55
42
F
p=0.0006
p= 0.16
p= 0.002
p=0.01
p=0.0006
% viability
Aβ
24h
48h
undifferentiated
RA/BDNF

Figure 1-2

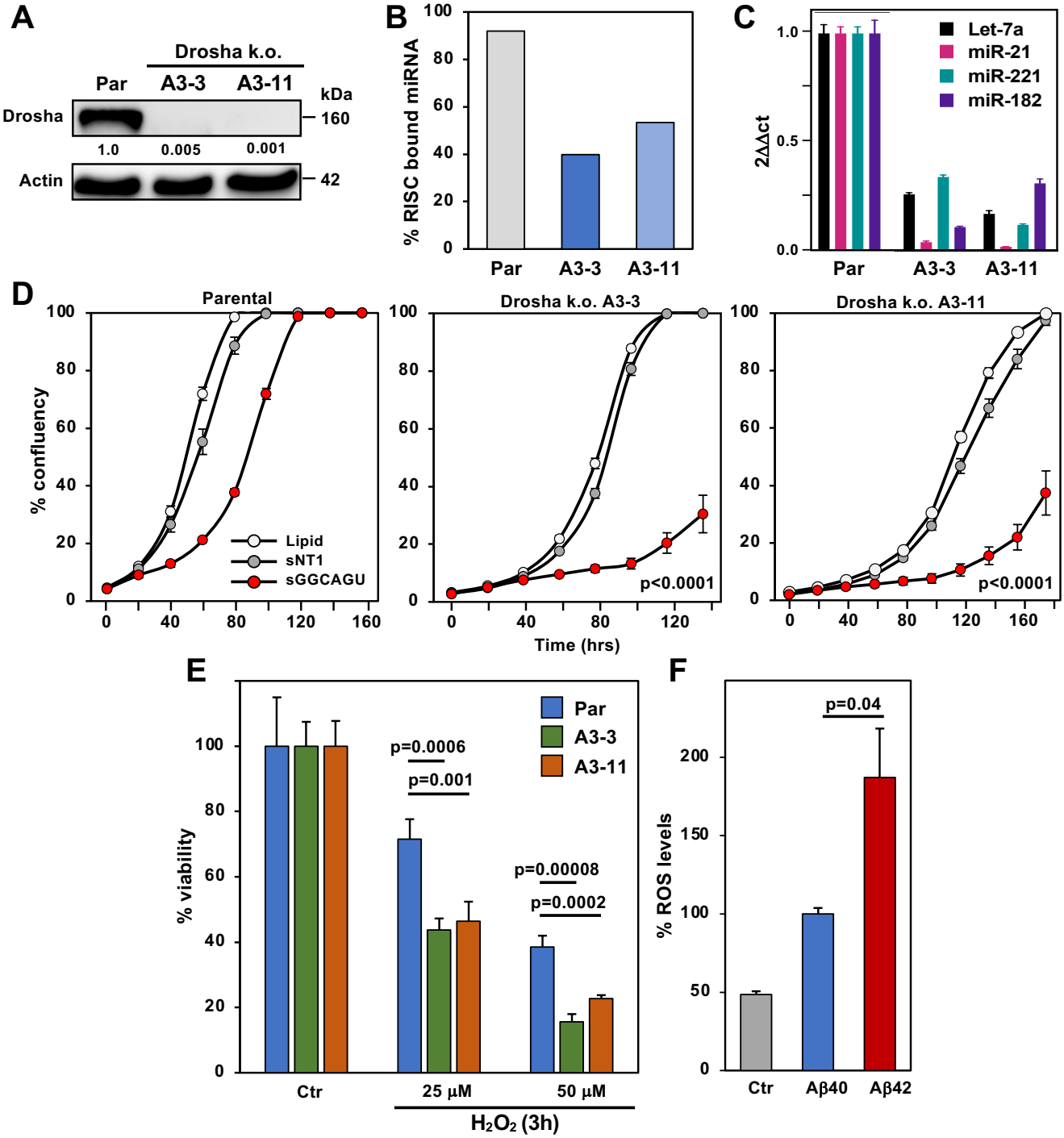
A
Drosha k.o.
Par
A3-3
A3-11
kDa
Drosha
160
1.0
0.005
0.001
Actin
42
B
% RISC bound miRNA
Par
A3-3
A3-11
C
2ΔΔct
Let-7a
miR-21
miR-221
miR-182
Par
A3-3
A3-11
D
Parental
Drosha k.o. A3-3
Drosha k.o. A3-11
% confluency
Lipid
sNT1
sGGCAGU
p<0.0001
p<0.0001
Time (hrs)
E
% viability
Par
A3-3
A3-11
p=0.0006
p=0.001
p=0.00008
p=0.0002
Ctr
25 μM
50 μM
H₂O₂ (3h)
F
% ROS levels
p=0.04
Ctr
Aβ40
Aβ42

Figure 1-3

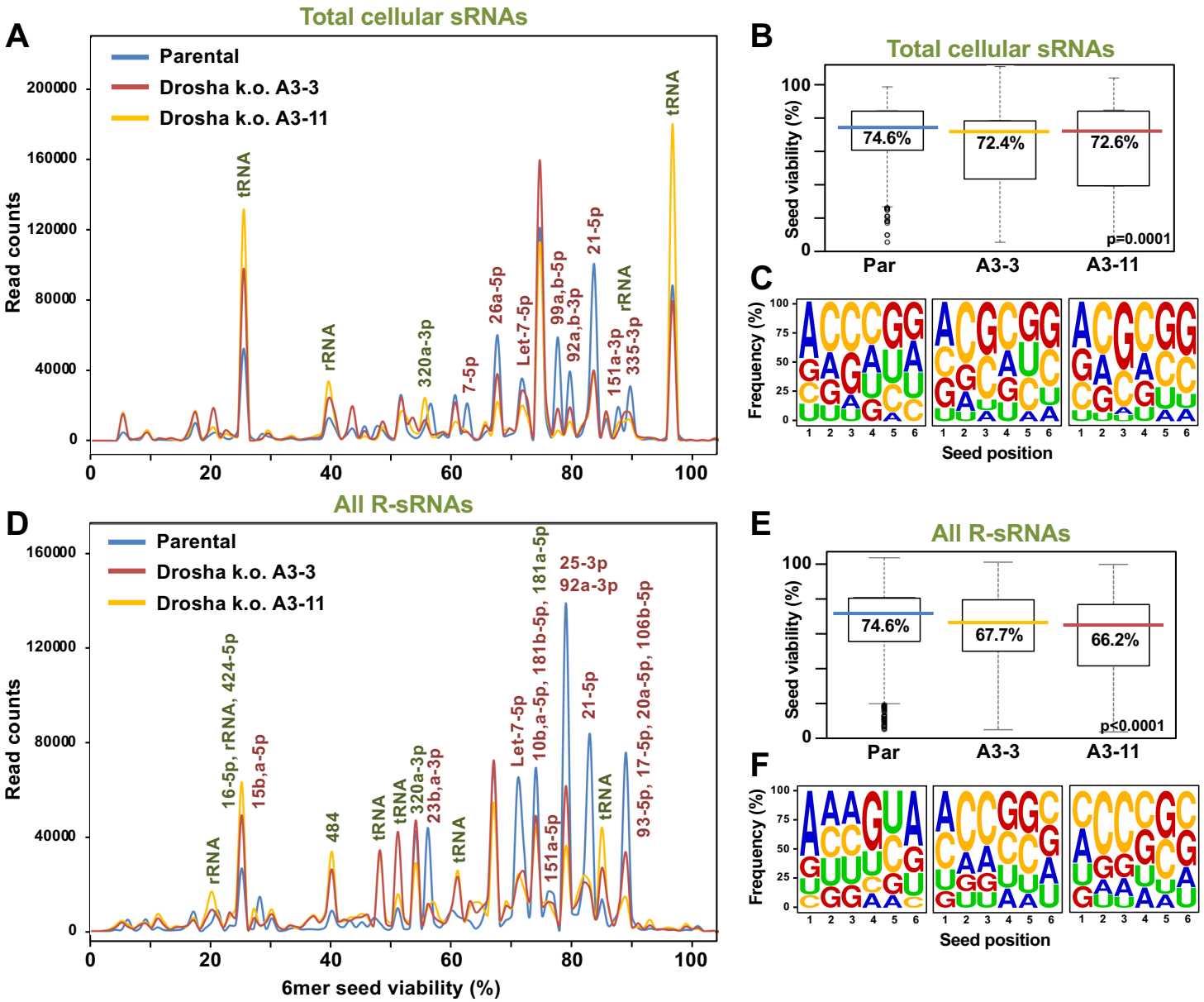
A
Total cellular sRNAs
Parental
Drosha k.o. A3-3
Drosha k.o. A3-11
Read counts
tRNA
rRNA
320a-3p
7-5p
26a-5p
Let-7-5p
99a,b-5p
92a,b-3p
21-5p
151a-3p
335-3p
rRNA
tRNA
B
Total cellular sRNAs
Seed viability (%)
74.6%
72.4%
72.6%
p=0.0001
Par
A3-3
A3-11
C
Frequency (%)
Seed position
D
All R-sRNAs
Parental
Drosha k.o. A3-3
Drosha k.o. A3-11
Read counts
rRNA
16-5p, rRNA, 424-5p
15b,a-5p
484
tRNA
tRNA
320a-3p
23b,a-3p
tRNA
Let-7-5p
10b,a-5p, 181b-5p, 181a-5p
151a-5p
25-3p
92a-3p
21-5p
tRNA
93-5p, 17-5p, 20a-5p, 106b-5p
6mer seed viability (%)
E
All R-sRNAs
Seed viability (%)
74.6%
67.7%
66.2%
p≤0.0001
Par
A3-3
A3-11
F
Frequency (%)
Seed position

Figure 1-4

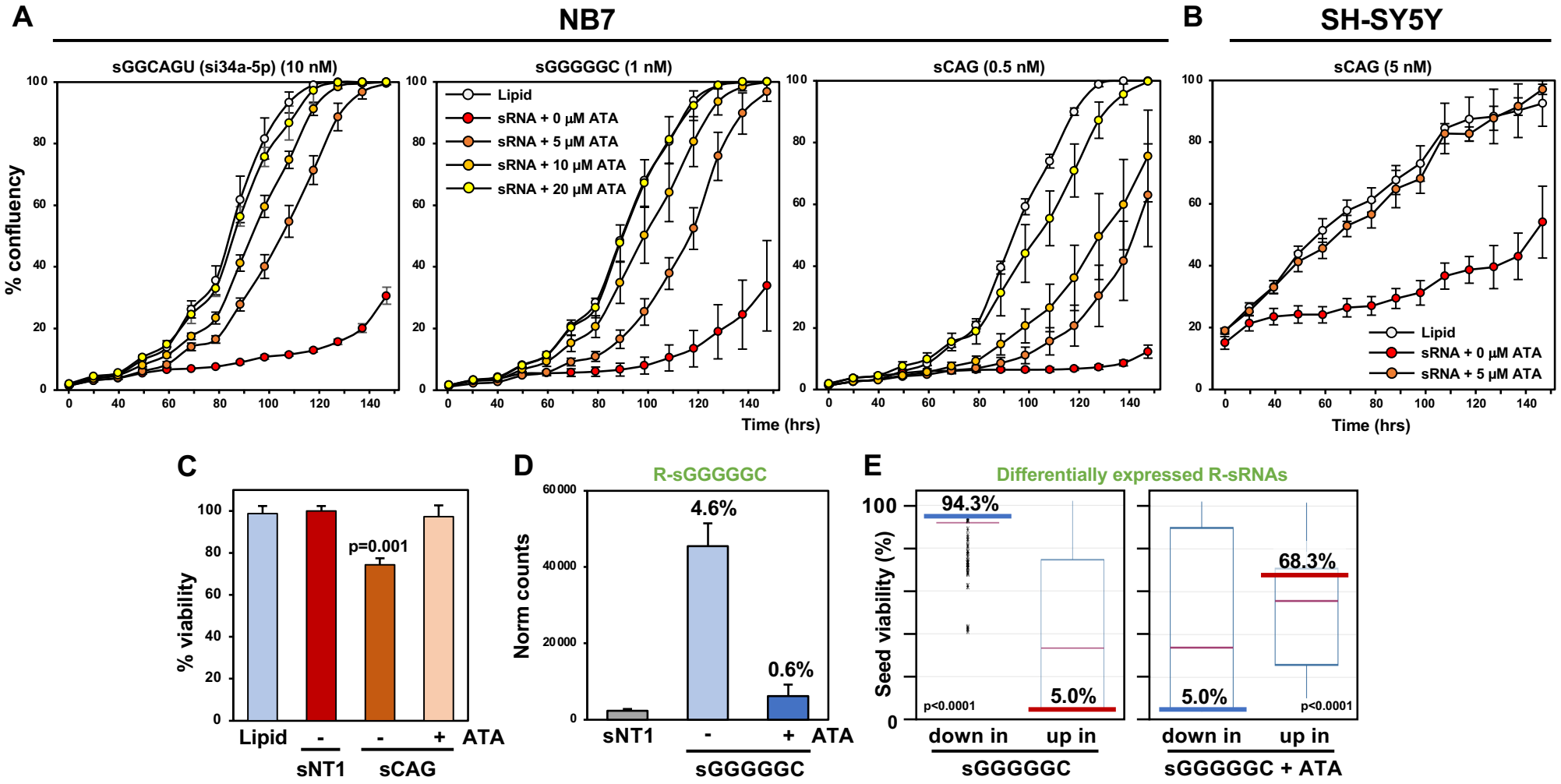
A
NB7
sGGCAGU (si34a-5p) (10 nM)
sGGGGGC (1 nM)
sCAG (0.5 nM)
% confluency
Time (hrs)
Lipid
sRNA + 0 µM ATA
sRNA + 5 µM ATA
sRNA + 10 µM ATA
sRNA + 20 µM ATA
B
SH-SY5Y
sCAG (5 nM)
Lipid
sRNA + 0 µM ATA
sRNA + 5 µM ATA
Time (hrs)
C
% viability
p=0.001
Lipid
-
-
+
ATA
sNT1
sCAG
D
R-sGGGGGC
Norm counts
4.6%
0.6%
sNT1
-
+
ATA
sGGGGGC
E
Differentially expressed R-sRNAs
Seed viability (%)
94.3%
5.0%
p<0.0001
68.3%
5.0%
p<0.0001
down in
up in
sGGGGGC
down in
up in
sGGGGGC + ATA

Figure 1-5

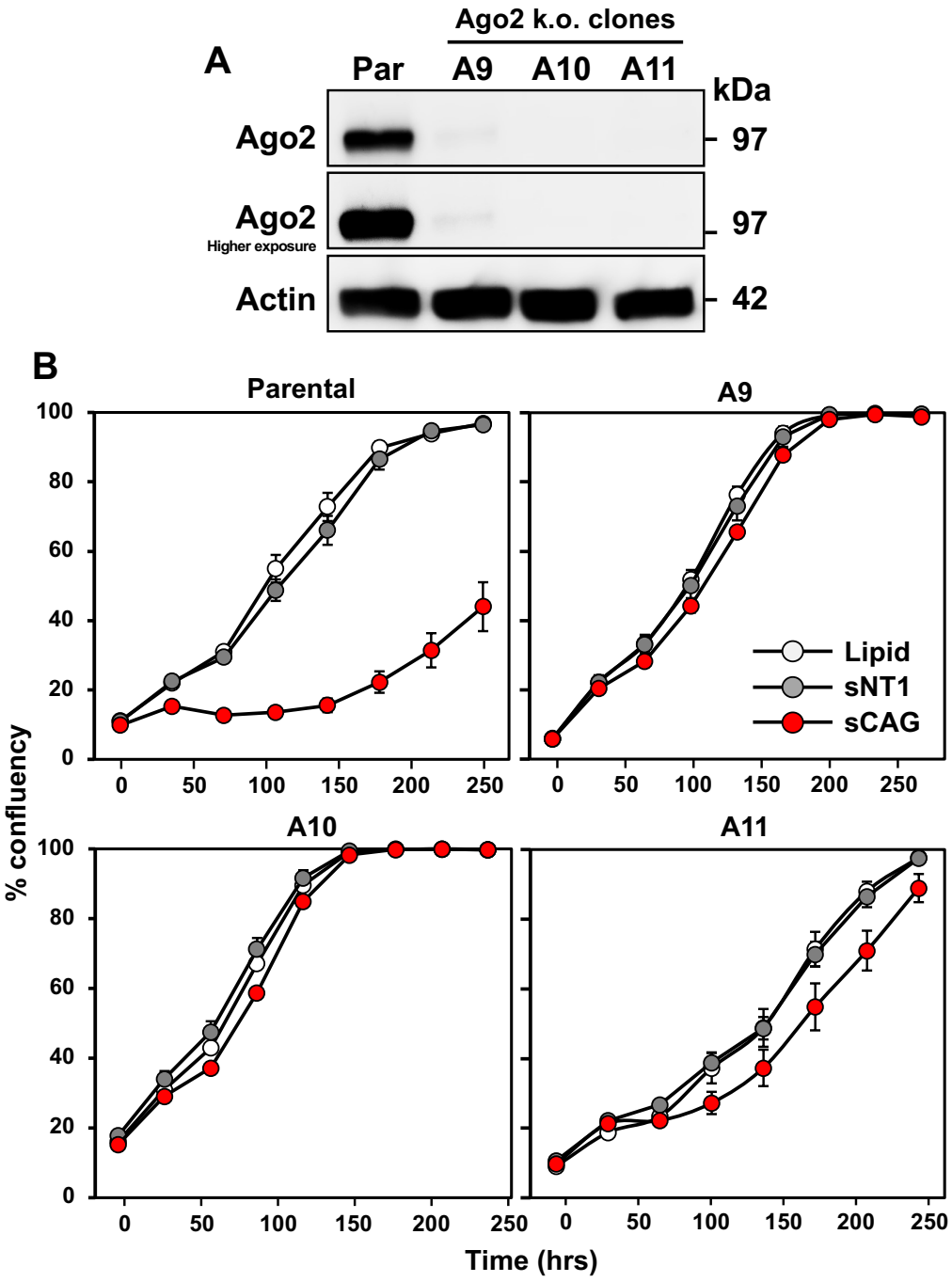
A
Ago2 k.o. clones
Par
A9
A10
A11
kDa
Ago2
97
Ago2
Higher exposure
97
Actin
42
B
Parental
A9
A10
A11
% confluency
Time (hrs)
Lipid
sNT1
sCAG

Figure 2

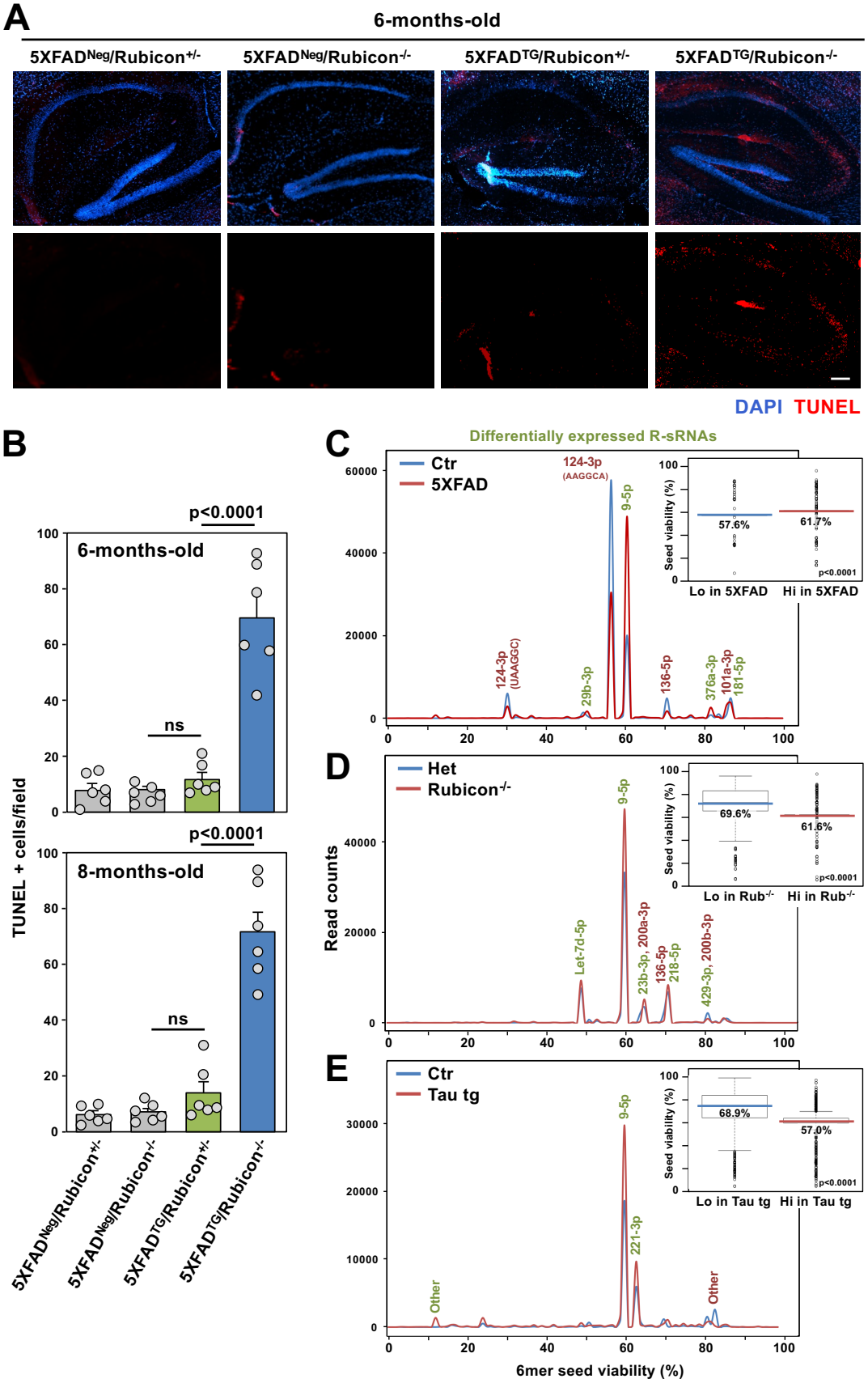
A
6-months-old
5XFAD^Neg/Rubicon^+/-
5XFAD^Neg/Rubicon^-/-
5XFAD^TG/Rubicon^+/-
5XFAD^TG/Rubicon^-/-
DAPI TUNEL
B
TUNEL + cells/field
6-months-old
8-months-old
p<0.0001
ns
C
Differentially expressed R-sRNAs
Ctr
5XFAD
124-3p (AAGGCA)
9-5p
124-3p (UAAGGC)
29b-3p
136-5p
376a-3p
101a-3p
181-5p
Seed viability (%)
57.6%
61.7%
Lo in 5XFAD
Hi in 5XFAD
D
Het
Rubicon-/-
Read counts
Let-7d-5p
23b-3p, 200a-3p
136-5p
218-5p
429-3p, 200b-3p
69.6%
61.6%
Lo in Rub-/-
Hi in Rub-/-
E
Ctr
Tau tg
221-3p
Other
68.9%
57.0%
Lo in Tau tg
Hi in Tau tg
6mer seed viability (%)

Figure 2-1

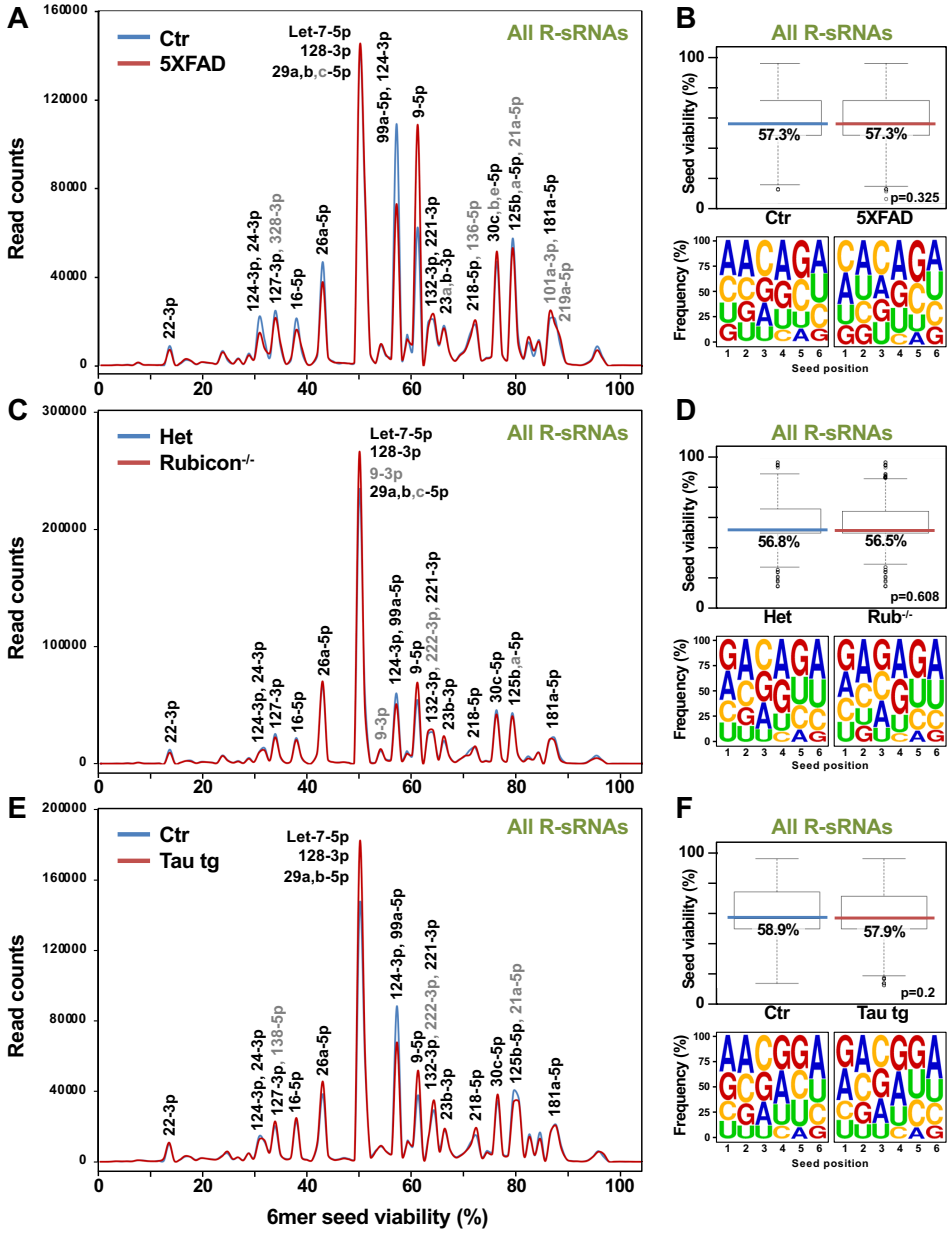
A
Ctr
5XFAD
All R-sRNAs
Read counts
Let-7-5p
128-3p
29a,b,c-5p
99a-5p, 124-3p
9-5p
22-3p
124-3p, 24-3p
127-3p, 328-3p
16-5p
26a-5p
132-3p, 221-3p
23a,b-3p
218-5p, 136-5p
30c,b,e-5p
125b,a-5p, 21a-5p
101a-3p, 181a-5p
219a-5p
B
All R-sRNAs
Seed viability (%)
57.3%
57.3%
p=0.325
Ctr
5XFAD
Frequency (%)
Seed position
C
Het
Rubicon-/-
All R-sRNAs
Read counts
Let-7-5p
128-3p
9-3p
29a,b,c-5p
22-3p
124-3p, 24-3p
127-3p
16-5p
26a-5p
9-3p
124-3p, 99a-5p
9-5p
132-3p, 222-3p, 221-3p
23b-3p
218-5p
30c-5p
125b,a-5p
181a-5p
D
All R-sRNAs
Seed viability (%)
56.8%
56.5%
p=0.608
Het
Rub-/-
Frequency (%)
Seed position
E
Ctr
Tau tg
All R-sRNAs
Read counts
Let-7-5p
128-3p
29a,b-5p
22-3p
124-3p, 24-3p
127-3p, 138-5p
16-5p
26a-5p
124-3p, 99a-5p
9-5p
132-3p, 222-3p, 221-3p
23b-3p
218-5p
30c-5p
125b-5p, 21a-5p
181a-5p
6mer seed viability (%)
F
All R-sRNAs
Seed viability (%)
58.9%
57.9%
p=0.2
Ctr
Tau tg
Frequency (%)
Seed position

Figure 3

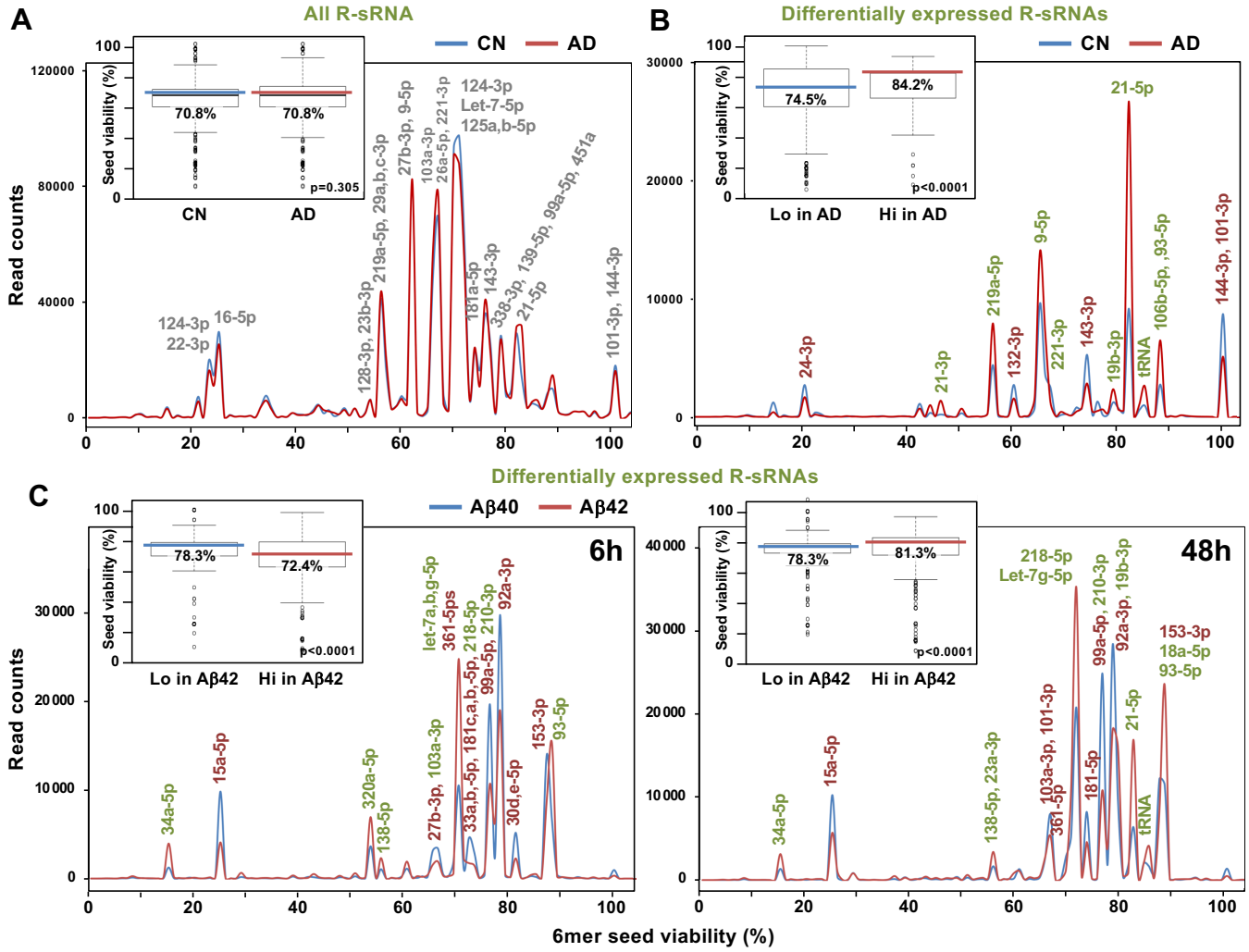
A
All R-sRNA
CN
AD
Read counts
Seed viability (%)
70.8%
70.8%
p=0.305
CN
AD
124-3p
22-3p
16-5p
128-3p, 23b-3p
219a-5p, 29a,b,c-3p
27b-3p, 9-5p
103a-3p
26a-5p, 221-3p
124-3p
Let-7-5p
125a,b-5p
181a-5p
143-3p
338-3p, 139-5p, 99a-5p, 451a
21-5p
101-3p, 144-3p
B
Differentially expressed R-sRNAs
CN
AD
74.5%
84.2%
p<0.0001
Lo in AD
Hi in AD
24-3p
21-3p
219a-5p
132-3p
9-5p
221-3p
143-3p
19b-3p
21-5p
tRNA
106b-5p, 93-5p
144-3p, 101-3p
C
Differentially expressed R-sRNAs
Aβ40
Aβ42
6h
78.3%
72.4%
p<0.0001
Lo in Aβ42
Hi in Aβ42
34a-5p
15a-5p
320a-5p
138-5p
27b-3p, 103a-3p
let-7a,b,g-5p
361-5ps
33a,b,-5p, 181c,a,b,-5p, 218-5p
99a-5p, 210-3p
92a-3p
30d,e-5p
153-3p
93-5p
48h
78.3%
81.3%
p<0.0001
Lo in Aβ42
Hi in Aβ42
34a-5p
15a-5p
138-5p, 23a-3p
103a-3p, 101-3p
361-5p
181-5p
218-5p
Let-7g-5p
99a-5p, 210-3p
92a-3p, 19b-3p
21-5p
tRNA
153-3p
18a-5p
93-5p
6mer seed viability (%)

Figure 3-1

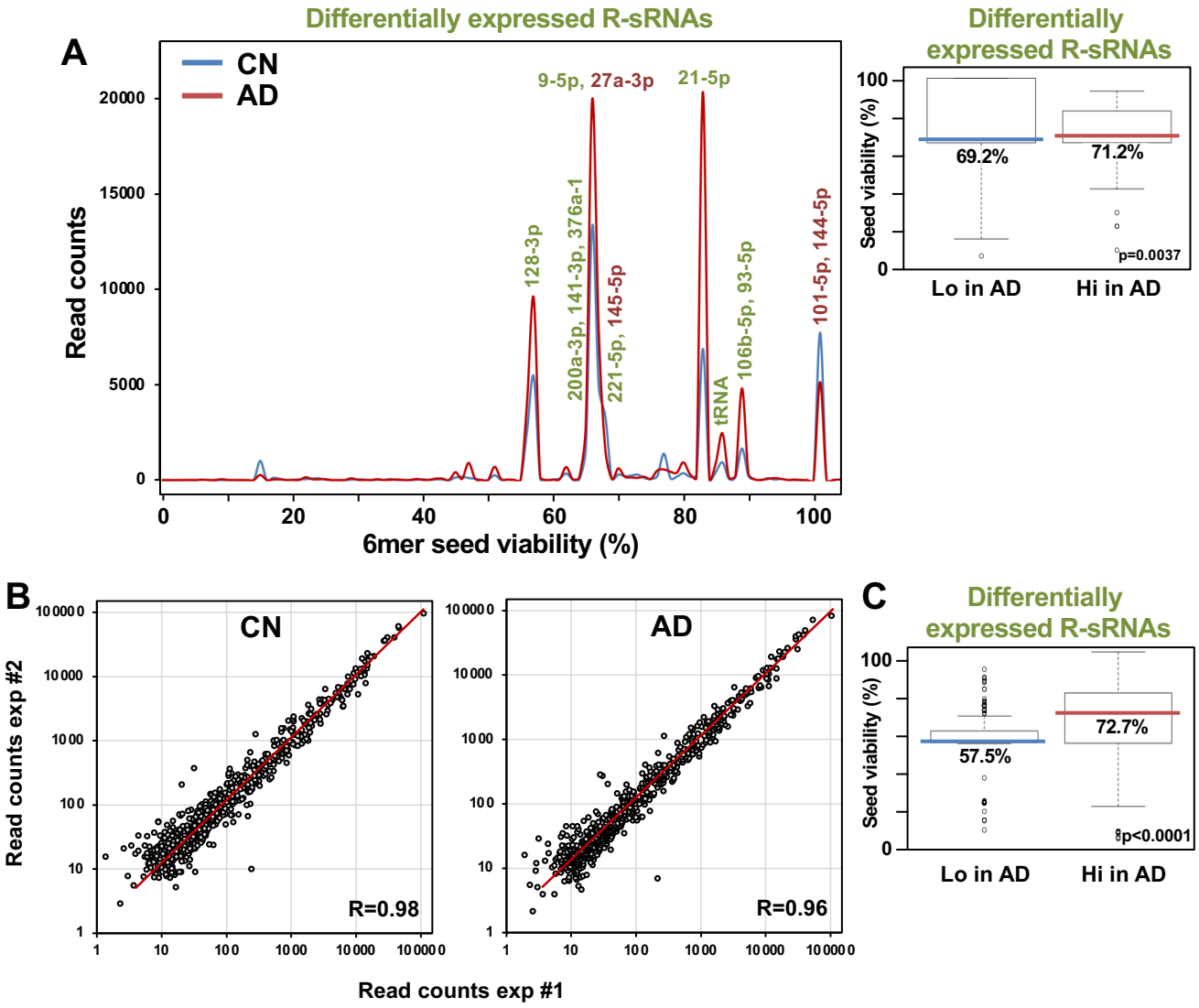
Differentially expressed R-sRNAs
A
CN
AD
Read counts
6mer seed viability (%)
128-3p
200a-3p, 141-3p, 376a-1
9-5p, 27a-3p
221-5p, 145-5p
21-5p
tRNA
106b-5p, 93-5p
101-5p, 144-5p
Differentially expressed R-sRNAs
Seed viability (%)
69.2%
71.2%
p=0.0037
Lo in AD
Hi in AD
B
CN
AD
Read counts exp #2
Read counts exp #1
R=0.98
R=0.96
C
Differentially expressed R-sRNAs
Seed viability (%)
57.5%
72.7%
p<0.0001
Lo in AD
Hi in AD

Figure 3-2

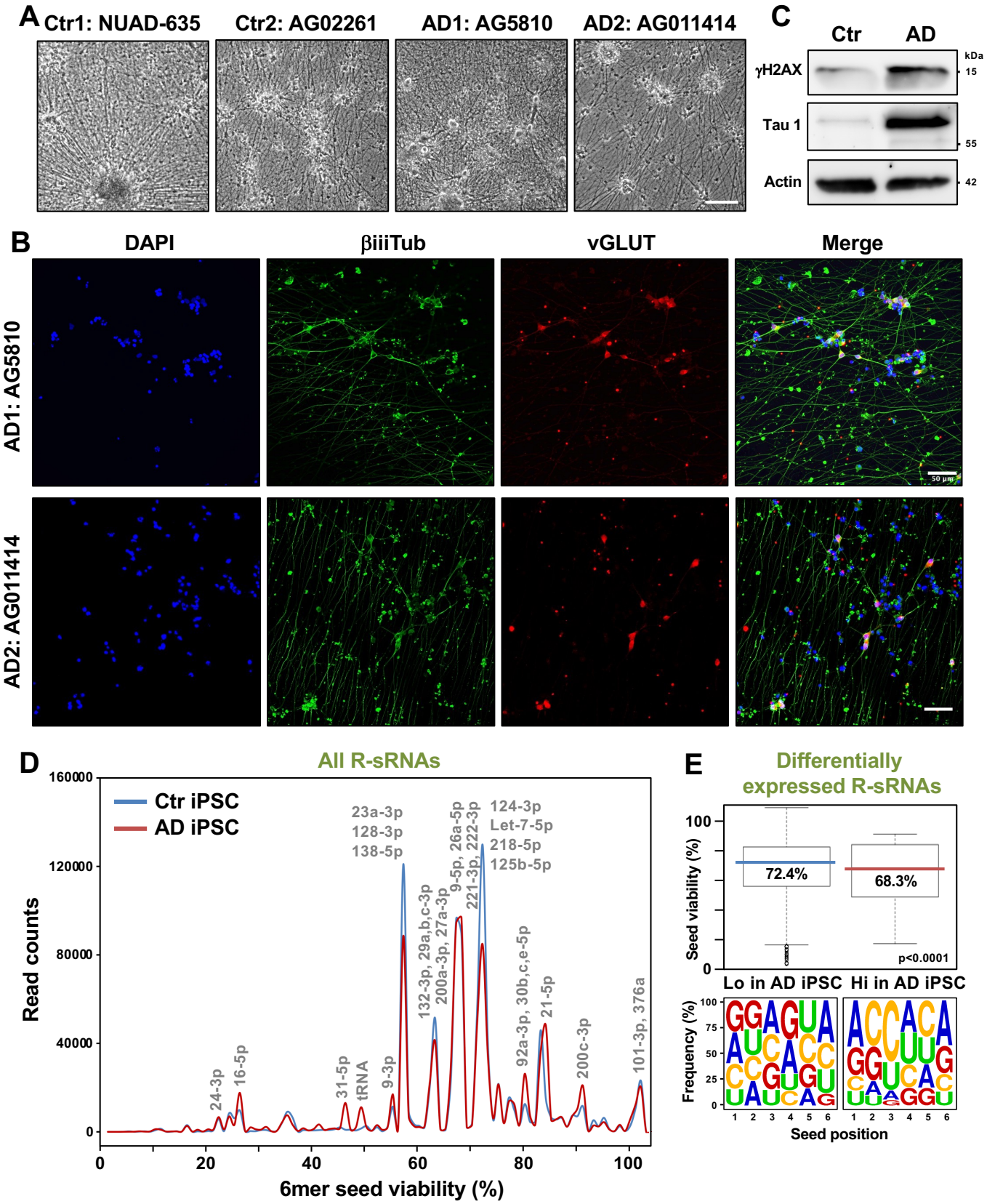
A
Ctr1: NUAD-635
Ctr2: AG02261
AD1: AG5810
AD2: AG011414
C
Ctr
AD
kDa
γH2AX
15
Tau 1
55
Actin
42
B
DAPI
βiiiTub
vGLUT
Merge
AD1: AG5810
AD2: AG011414
50 µm
D
All R-sRNAs
Ctr iPSC
AD iPSC
Read counts
6mer seed viability (%)
24-3p
16-5p
31-5p
tRNA
9-3p
23a-3p
128-3p
138-5p
132-3p, 29a,b,c-3p
200a-3p, 27a-3p
9-5p, 26a-5p
221-3p, 222-3p
124-3p
Let-7-5p
218-5p
125b-5p
92a-3p, 30b,c,e-5p
21-5p
200c-3p
101-3p, 376a
E
Differentially expressed R-sRNAs
Seed viability (%)
72.4%
68.3%
p<0.0001
Lo in AD iPSC
Hi in AD iPSC
Frequency (%)
Seed position

Figure 3-3

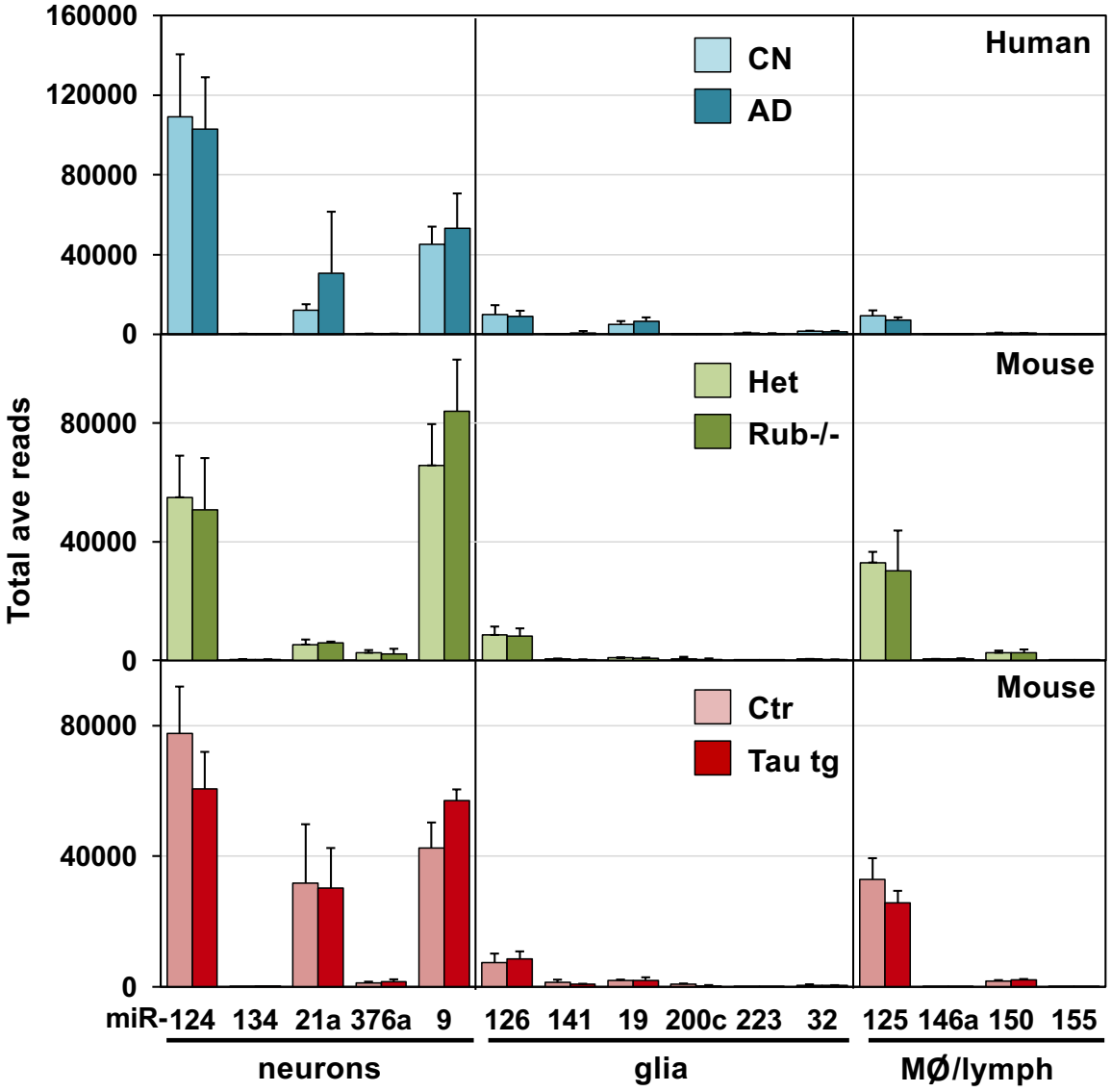
Total ave reads
160000
120000
80000
40000
0
CN
AD
Human
Het
Rub-/-
Mouse
Ctr
Tau tg
Mouse
miR-124 134 21a 376a 9 126 141 19 200c 223 32 125 146a 150 155
neurons
glia
MØ/lymph

Table 3-1

	ID	Region	ApoE	Age	Disease Duration (y)	Gender	PMI	Race	Clinical Diagnosis	Br wt	Pathologic Diagnosis
Controls											
	CN1	T		76		F	13	C	CN	950Fr	Low ADNC
	CN2	O		81		M	12	C	CN	1310Fr	Low ADNC
	CN3	T		83		F	43	C	CN	1240Fr	Low ADNC
	CN4	T & F		87		M	16	C	CN	1400Fr	Intermediate ADNC
	CN5	T & F		100		F	14	C	CN	1000Fr	Intermediate ADNC
Average				85.4			19.6				
AD											
	AD1	T & F	3,3	74	8	M	21	C	AD	1320Fr	High ADNC
	AD2	T & F	3,4	77	14	F	21	C	AD	1040Fr	High ADNC
	AD3	T & F	3,4	81	5	M	19	C	AD	1340Fr	High ADNC
	AD4	T & F	3,4	83	3	F	24	C	AD	1330Fr	High ADNC
	AD5	T & F	3,4	83	11	M	12	C	AD	1240Fr	High ADNC
	AD6	T & F	3,4	89	13	F	71	C	AD	980Fr	High ADNC
	AD7	T & F	3,4	93	12	M	10	C	AD	1180Fr	High ADNC
Average				82.9	9		25.4				
SuperAgers		**Region**		**Age**		**Gender**	**PMI**	**Race**	**Clinical Dx**	**Weight**	**Pathologic Diagnosis-1**
	SA1	F		90		M	14	C	CN (SA)	1267Fr	Low ADNC
	SA2	F		85		Fe	9	C	CN (SA)	1310Fr	Low ADNC Tau Only
	SA3	F		82		Fe	24	C	CN (SA)	1241Fr	Low ADNC
Average				85.7			15.7				

Figure 4

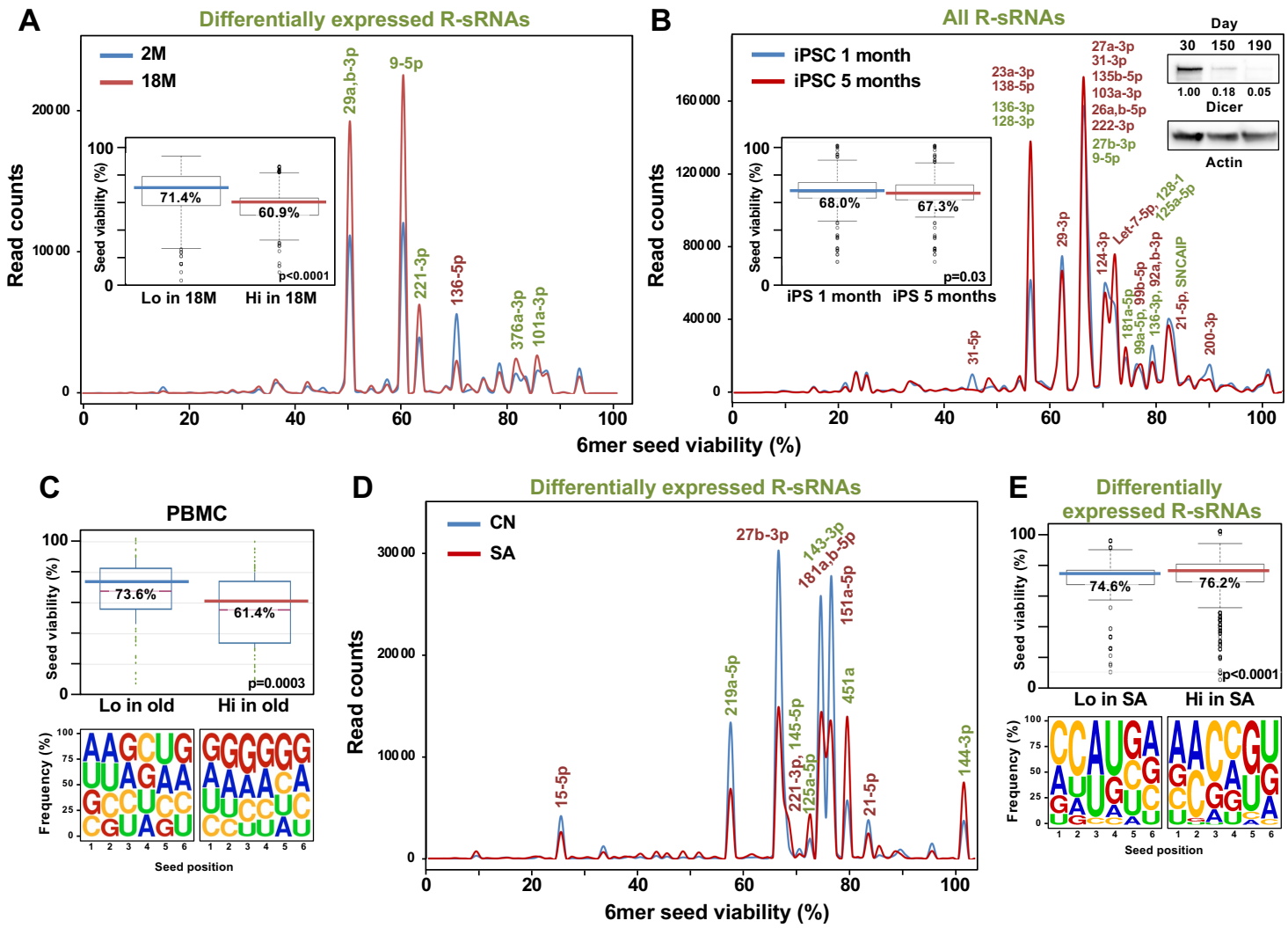
A
Differentially expressed R-sRNAs
2M
18M
Read counts
Seed viability (%)
71.4%
60.9%
p<0.0001
Lo in 18M
Hi in 18M
29a,b-3p
9-5p
221-3p
136-5p
376a-3p
101a-3p
6mer seed viability (%)
B
All R-sRNAs
iPSC 1 month
iPSC 5 months
Day
30 150 190
1.00 0.18 0.05
Dicer
Actin
68.0%
67.3%
p=0.03
iPS 1 month
iPS 5 months
23a-3p
138-5p
136-3p
128-3p
27a-3p
31-3p
135b-5p
103a-3p
26a,b-5p
222-3p
27b-3p
9-5p
29-3p
124-3p
Let-7-5p, 128-1
125a-5p
181a-5p
99a-5p, 99b-5p
136-3p, 92a,b-3p
21-5p, SNCAIP
200-3p
31-5p
C
PBMC
73.6%
61.4%
p=0.0003
Lo in old
Hi in old
Frequency (%)
Seed position
D
Differentially expressed R-sRNAs
CN
SA
27b-3p
143-3p
181a,b-5p
151a-5p
219a-5p
451a
145-5p
221-3p,
125a-5p
21-5p
15-5p
144-3p
E
Differentially expressed R-sRNAs
74.6%
76.2%
p<0.0001
Lo in SA
Hi in SA

Figure 4-1

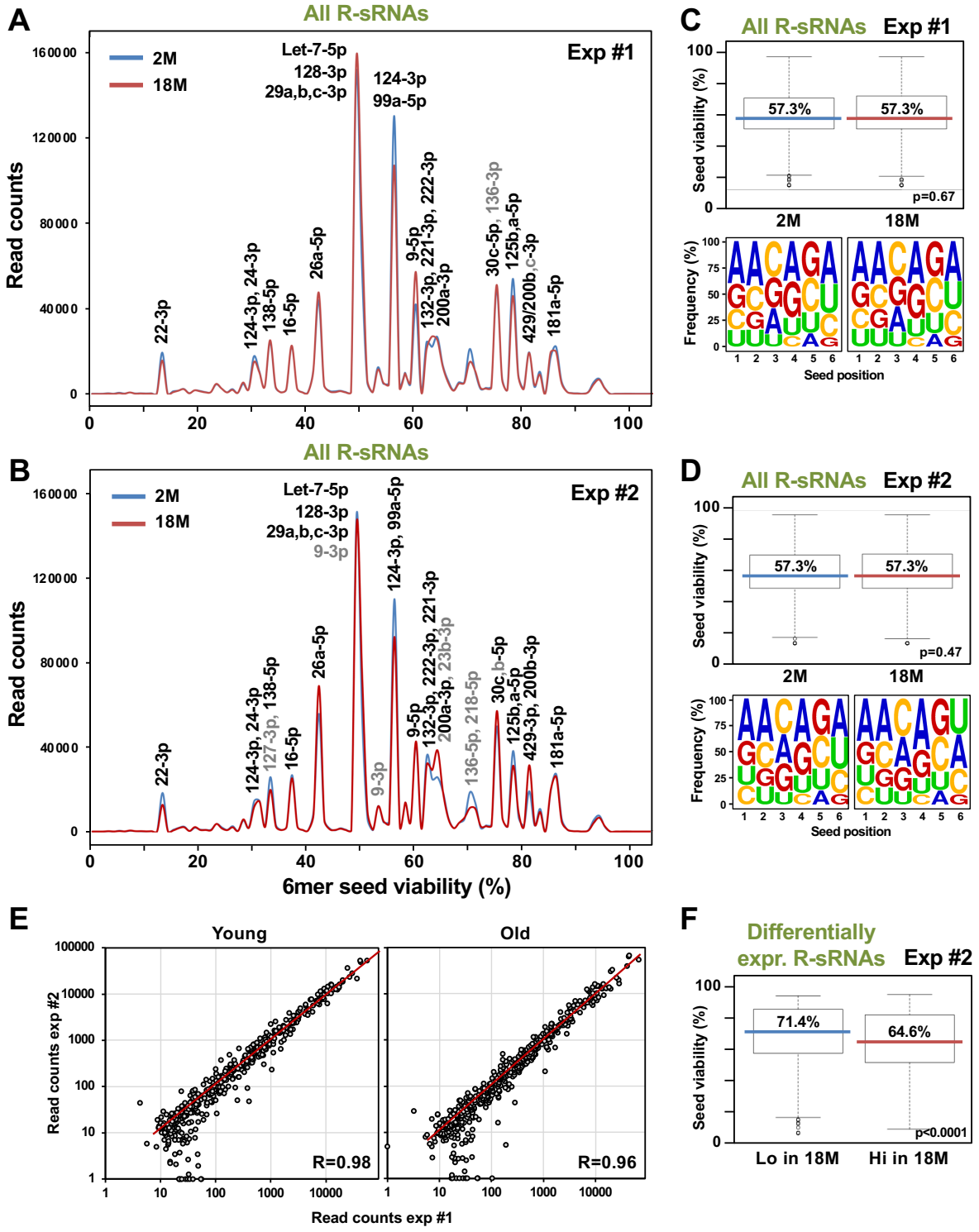
A
All R-sRNAs
Exp #1
2M
18M
Read counts
Let-7-5p
128-3p
29a,b,c-3p
124-3p
99a-5p
22-3p
124-3p, 24-3p
138-5p
16-5p
26a-5p
9-5p
132-3p, 221-3p, 222-3p
200a-3p
30c-5p, 136-3p
125b,a-5p
429/200b,c-3p
181a-5p
B
All R-sRNAs
Exp #2
Let-7-5p
128-3p
29a,b,c-3p
9-3p
124-3p, 99a-5p
22-3p
124-3p, 24-3p
127-3p, 138-5p
16-5p
26a-5p
9-3p
9-5p
132-3p, 221-3p
222-3p, 23b-3p
200a-3p
136-5p, 218-5p
30c,b-5p
125b,a-5p
429-3p, 200b-3p
181a-5p
6mer seed viability (%)
C
All R-sRNAs Exp #1
Seed viability (%)
57.3%
57.3%
p=0.67
2M
18M
Frequency (%)
Seed position
D
All R-sRNAs Exp #2
Seed viability (%)
57.3%
57.3%
p=0.47
2M
18M
Frequency (%)
Seed position
E
Young
Old
Read counts exp #2
R=0.98
R=0.96
Read counts exp #1
F
Differentially expr. R-sRNAs Exp #2
Seed viability (%)
71.4%
64.6%
p<0.0001
Lo in 18M
Hi in 18M

Figure 4-2

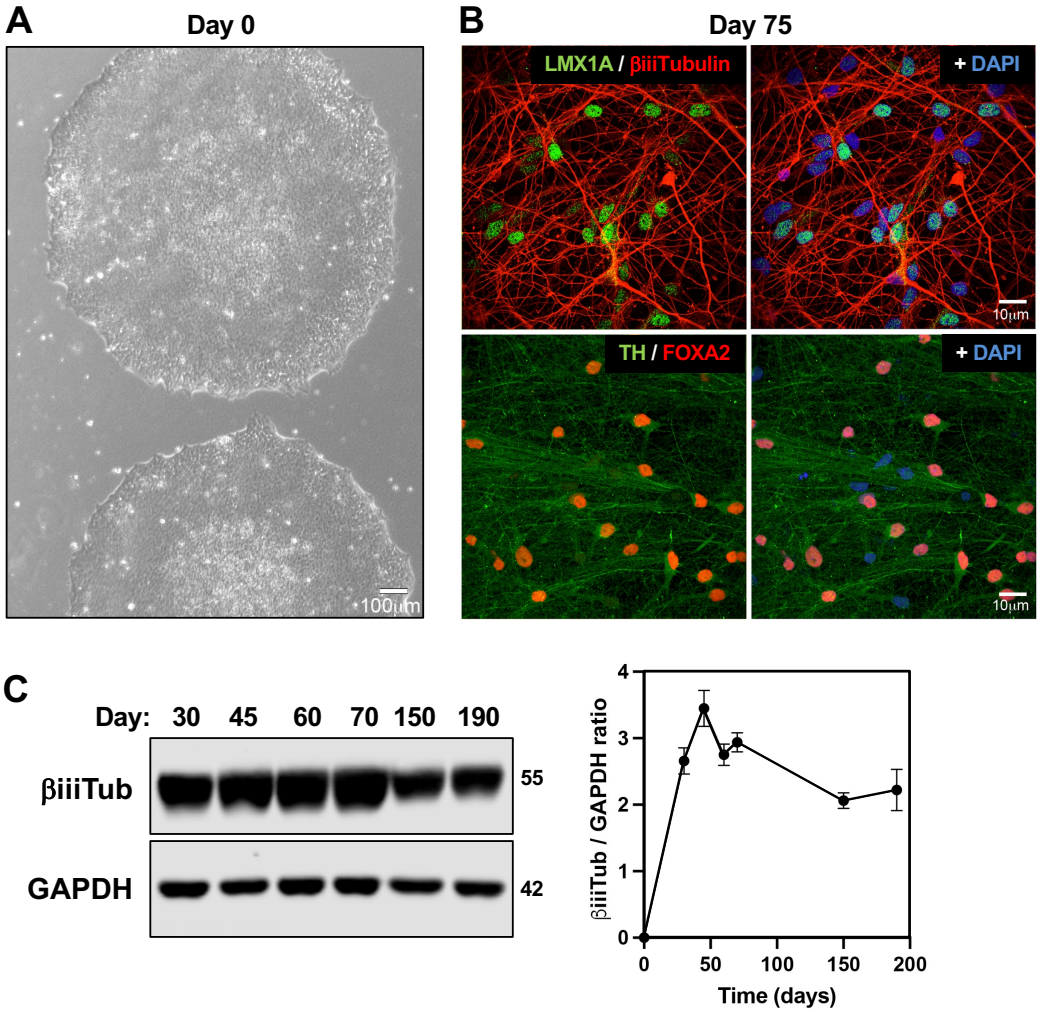
A
Day 0
100µm
B
Day 75
LMX1A / βiiiTubulin
+ DAPI
10µm
TH / FOXA2
+ DAPI
10µm
C
Day: 30 45 60 70 150 190
βiiiTub
55
GAPDH
42
βiiiTub / GAPDH ratio
0
1
2
3
4
0
50
100
150
200
Time (days)

Figure 4-3

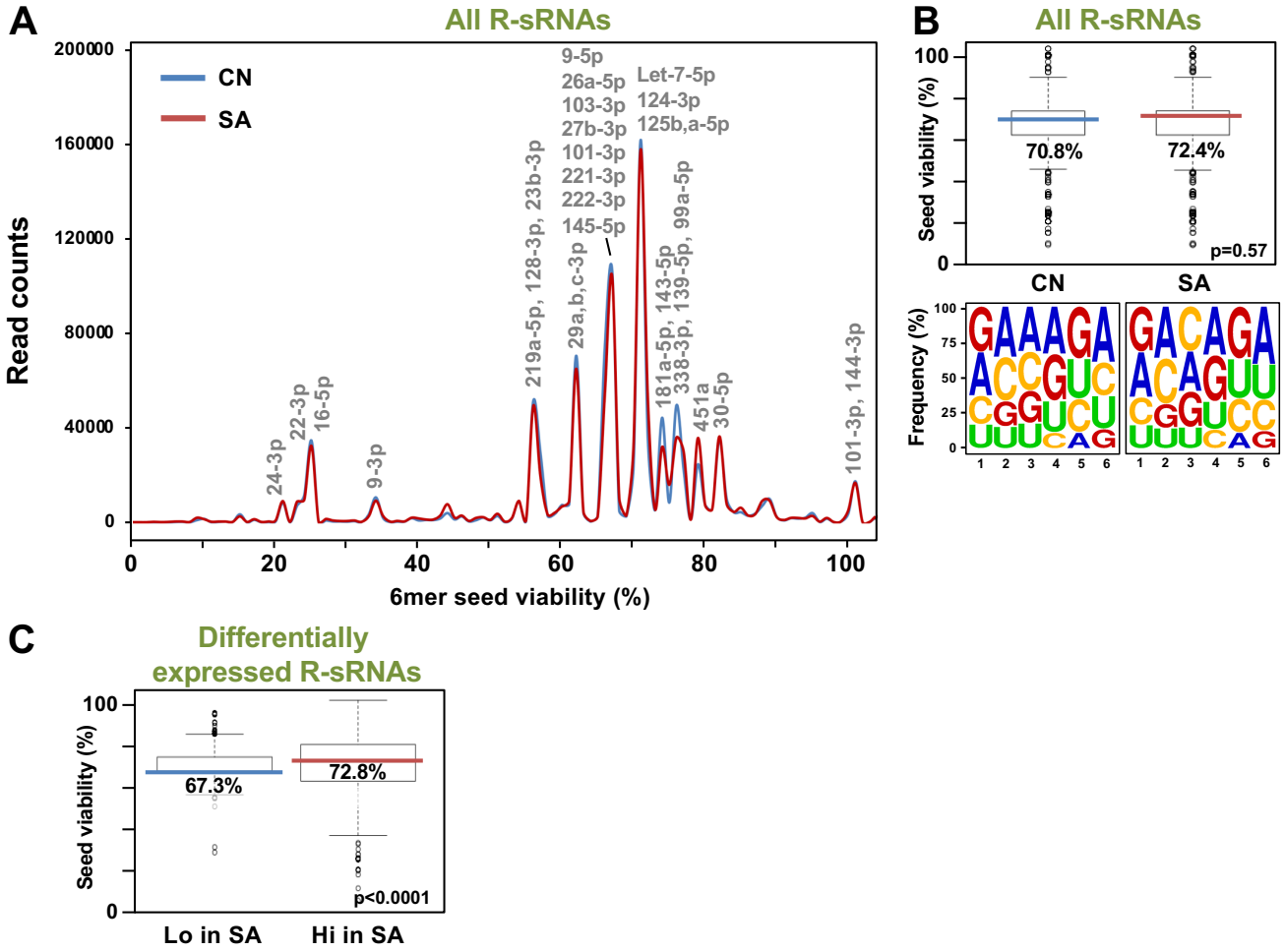
A
All R-sRNAs
CN
SA
Read counts
200000
160000
120000
80000
40000
0
24-3p
22-3p
16-5p
9-3p
219a-5p, 128-3p, 23b-3p
29a,b,c-3p
9-5p
26a-5p
103-3p
27b-3p
101-3p
221-3p
222-3p
145-5p
Let-7-5p
124-3p
125b,a-5p
181a-5p, 143-5p
338-3p, 139-5p, 99a-5p
451a
30-5p
101-3p, 144-3p
0
20
40
60
80
100
6mer seed viability (%)
B
All R-sRNAs
Seed viability (%)
100
0
70.8%
72.4%
p=0.57
CN
SA
Frequency (%)
100
75
50
25
0
1 2 3 4 5 6
1 2 3 4 5 6

C
Differentially expressed R-sRNAs
Seed viability (%)
100
0
67.3%
72.8%
p<0.0001
Lo in SA
Hi in SA

Figure 5

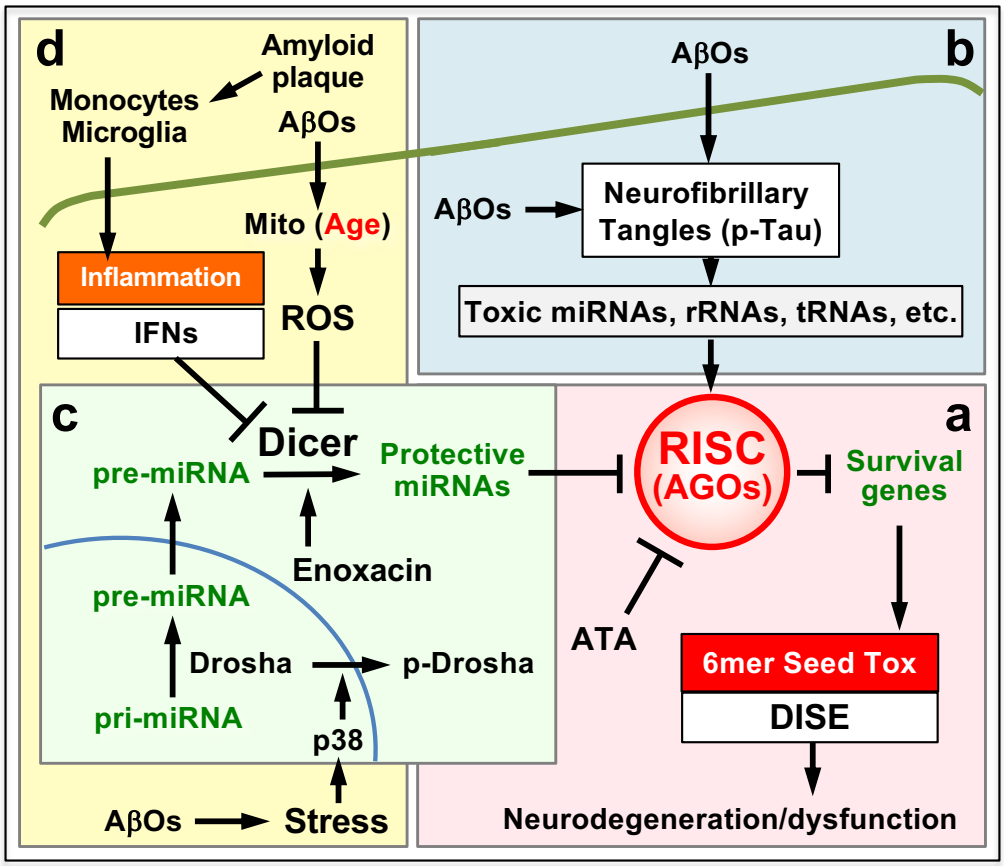
d
Amyloid plaque
Monocytes Microglia
AβOs
Mito (Age)
Inflammation
IFNs
ROS
b
AβOs
AβOs
Neurofibrillary Tangles (p-Tau)
Toxic miRNAs, rRNAs, tRNAs, etc.
c
Dicer
pre-miRNA
Protective miRNAs
Enoxacin
pre-miRNA
Drosha
p-Drosha
pri-miRNA
p38
AβOs
Stress
a
RISC (AGOs)
Survival genes
ATA
6mer Seed Tox
DISE
Neurodegeneration/dysfunction